

Orbital Stability Zones about Asteroids

II. The Destabilizing Effects of Eccentric Orbits and of Solar Radiation

DOUGLAS P. HAMILTON AND JOSEPH A. BURNS

Cornell University, Ithaca, New York

Received October 28, 1991; revised December 18, 1991

The gravitational effects of the Sun on a particle orbiting another massive body which itself moves on a circular path around the Sun have been studied extensively. Most recently, D. P. Hamilton and J. A. Burns (1991, *Icarus* 92, 118–131) characterized the size and shape of a stability zone around an asteroid on a circular heliocentric orbit within which material could remain bound for an extended period of time. We now consider two additional effects analytically and numerically: the asteroid's nonzero heliocentric eccentricity and solar radiation pressure. In both of these cases, our numerical integrations apply directly to a spherical asteroid, "Amphitrite," with semimajor axis 2.55 AU, radius $R_A = 100$ km, and density 2.38 g/cm^3 . For an asteroid on an *eccentric* orbit we argue, based on numerical integrations and analytical approximations, that the stability zone scales roughly as the size of the Hill sphere calculated at the asteroid's pericenter. This scaling holds for large values of eccentricity and allows results for one asteroid with a given mass, semimajor axis, and eccentricity to be used for another with different values of these parameters. We compare predictions of the scaling law to numerical integrations for an "Amphitrite" with various orbital eccentricities and find good agreement for prograde orbits and for those with orbital planes nearly normal to the asteroid's heliocentric path, but not for retrograde orbits. We apply our results to the minor planet 951 Gaspra.

We also determine that solar radiation pressure is a very efficient mechanism for removing relatively small particles from the circumasteroidal zone. Radiation pressure acting on an orbiting grain can cause large oscillations in the grain's orbital eccentricity which in turn can lead to either escape from the system or impact with the asteroid. We find numerically that particles with radius 0.1 mm started on circular orbits escape from "Amphitrite" at all distances beyond $130 R_A$. Grains of this size started anywhere between the asteroid's surface and $130 R_A$ are forced to crash into the minor planet; smaller grains are even more severely affected. The orbits of millimeter-sized grains are also strongly perturbed. Planar paths bound for 20 years are found to extend to only $\sim 40\%$ of the critical distance found by Hamilton and Burns (1991); orbits with inclinations near 90° are somewhat more resilient. In all cases, orbital evolution occurs on time scales comparable to the asteroid's orbital period. Particles larger than a few centimeters are only

slightly affected by radiation pressure. These results can be applied to "Gaspra," an asteroid only one-thousandth as massive as "Amphitrite," by increasing all particle sizes by a factor of ~ 10 . © 1992 Academic Press, Inc.

1. INTRODUCTION

While two questions—"How much material is likely to be in orbit around an asteroid?" and "Exactly where will that material be?"—are interesting to planetary scientists and celestial mechanicians, they are critically important to those spacecraft mission planners who must decide how closely to approach such objects. It is well known that, in the absence of perturbations, orbiting particles can move on Keplerian paths at all distances from an isolated asteroid. In reality, however, gravitational perturbations from the Sun and other bodies, and solar radiation pressure will limit the zone in which particles can stably orbit.

The primary gravitational perturbation is from the Sun so, to first order, one can ignore other effects and look only at solar perturbations on a particle orbiting an asteroid which in turn orbits the Sun. The problem is greatly simplified if the orbits of the asteroid and the particle are coplanar and if the asteroid moves along a circular path about the Sun. In this case there are only two orbital types: *prograde* (those whose angular velocities are in the same sense as the asteroid's) and *retrograde* (those whose angular velocities are in the opposite sense). This problem was addressed by Zhang and Innanen (1988) who also looked briefly at an asteroid on a mildly eccentric orbit. Since then several studies have considered additional complications. Hamilton and Burns (1991) relaxed the restriction that the motion be confined to the asteroid's orbital plane and introduced the concept of a three-dimensional stability surface. Chauvineau and Mignard treated Jovian perturbations (1990b) and the disruption of a binary

asteroid by the close approach of other asteroids (Chauvineau *et al.* 1991). In the current paper we discuss two further effects, each of which acts in times comparable to the asteroid's orbital period. First, we present some analytic results and extensive numerical integrations for the eccentric three-dimensional problem. In the final section we discuss the influence of radiation pressure which, because of the asteroid's low gravity, is found to be surprisingly effective in removing millimeter- and centimeter-sized particles from circumasteroidal orbits. A synopsis of possible sources of circumasteroidal debris and of all the above-mentioned destabilizing effects can be found in Burns and Hamilton (1992).

1.1. Stability Surface for an Asteroid with Zero Eccentricity

We start by briefly summarizing the pertinent results of Hamilton and Burns (1991, henceforth HB1), who investigated the stability of orbits around a minor planet in the context of the three-body problem consisting of an asteroid, the Sun, and an infinitesimal test particle placed near the asteroid. Since the Sun's mass is much greater than the asteroid's, which in turn is much greater than that of the test particle, this problem is a limiting case of both Hill's problem (two small objects with a small separation orbiting a massive object) and the restricted three-body problem (a particle influenced by, but not influencing, a pair of much larger objects) (Hénon and Petit 1986). In our earlier study, we placed the asteroid on a circular orbit and studied trajectories of a test particle, normally in a reference frame centered on the asteroid and rotating with the asteroid's constant angular rate Ω around the Sun. The test particle began along the Sun-asteroid line on a path that would be circular in the Sun's absence, and could be inclined at an angle i from the asteroid's orbital plane; our two free parameters were therefore the particle's initial distance from the asteroid and its starting inclination.

The main goal of HB1 was to delineate a zone around an asteroid in which it would be possible to find bound, orbiting material, and hence our study focused on distant orbits that were very weakly linked to the asteroid. To accomplish this end, we looked at the orbits resulting from numerical integrations of the equations of motion for several thousand different initial conditions. Holding inclination constant, we found that increasing the initial distance of our test particle resulted in an abrupt transition between bound and unbound orbits occurring at a position we defined as the *critical distance*. Most grains started within the critical distance are tied to the asteroid, while most beginning outside of this distance escape, although there are exceptions as are seen below. The critical distance is a strong function of inclination, increasing for our

TABLE I
Parameters Used for "Amphitrite" and "Gaspra"

	a (AU)	e	Radius (km)	ρ (g/cm ³)	Hill radius (R_A)
"Amphitrite"	2.55	0.0	100	2.38	452
"Gaspra"	2.2	0.17	10	2.38	390

asteroid "Amphitrite" (parameters given in Table I) from approximately $220 R_A$ (asteroid radii) for prograde orbits to about $445 R_A$ for retrograde ones (see Fig. 15 of HB1). We then defined the three-dimensional stability surface to be the outer envelope encompassing all orbits corresponding to initial conditions which lie below the critical distance.

In order to study the large number of initial conditions necessary to adequately define the stability surface, we only followed individual particles for five orbits of the asteroid around the Sun or about 20 years. At first sight the short integration time might seem prohibitively restrictive for drawing conclusions on the long-term stability of circumasteroidal orbits, but we found that the critical distance, and hence the stability surface, was not very sensitive to differences in integration times. Indeed, for prograde orbits, escapes occur in less than 20 years for initial orbital distances within one asteroid radius of the position where the opening of the zero-velocity surfaces (or zero-velocity curves—ZVCs) first allows escape, a difference of less than 0.5% (see HB1 or Danby (1988) for a discussion of ZVCs; Lundberg *et al.* (1985) show nice three-dimensional views of these surfaces for the restricted three-body problem). Retrograde orbits, which are found to be stable far beyond the distance where the ZVCs first open (Chauvineau and Mignard 1990a), also seem to be relatively insensitive to differences in integration time; for a small subset of our numerical experiments in which orbits were followed for 1000 years, we found critical distances that differ by less than 1% from those obtained in 20-year integrations. Nevertheless, recent results from dynamical theory caution that additional escapes may occur without much forewarning when the integration time is increased; at any rate our results certainly overestimate the maximum possible extent of circumasteroidal debris.

The upper half of the stability zone within which debris is bound is shown in Fig. 16 of HB1. The zone is roughly spherical for latitudes less than 35° and has a radius slightly larger than the radius of the Hill sphere; this bounding distance is determined by the characteristic size of the largest retrograde orbit since such orbits are always the most stable. At higher latitudes, the stability zone is approximately flat and parallel to the asteroid's orbital plane at a height of about $2/3$ of the Hill radius. This flattened part of the stability surface is caused by orbits

with inclinations in the range $60^\circ < i < 120^\circ$ which were shown to rise to roughly the same height over much of the asteroid's orbital plane. HB1 argue that, for appropriate initial conditions, sizes of the stability surface can be scaled in proportion to the dimensions of the Hill sphere.

1.2. Coriolis Acceleration

We now discuss the Coriolis acceleration, the term $-2\mathbf{\Omega} \times \mathbf{v}_{\text{rot}}$ that appears when Newton's equation is written for a particle moving with velocity \mathbf{v}_{rot} relative to a reference frame rotating at angular velocity $\mathbf{\Omega}$. This slight diversion is made because we will often call upon Coriolis effects to explain differences in the stability of prograde and retrograde orbits; yet the role of the Coriolis acceleration in determining whether an orbit will remain bound may be puzzling because the Coriolis acceleration does no work and hence does not change the orbit's "energy" as calculated in the rotating frame. In the following paragraphs, we explain in detail how the Coriolis acceleration influences the stability of an orbit.

In dynamics, the Coriolis and centrifugal accelerations have always had somewhat tarnished reputations, often dismissed as merely "fictitious" accelerations conjured up to explain differences between motions observed in a rotating frame and the predictions of Newton's $\mathbf{F} = m\mathbf{a}$ written in that frame. Of the two, the Coriolis acceleration is considered to be the most mysterious and least reputable since, unlike the centrifugal acceleration, it cannot be derived from a potential. While it is strictly true that these accelerations are "fictitious," the air of illegitimacy that accompanies them is undeserved since their inclusion in the equations of motion is a perfectly valid way to treat a given dynamics problem. Indeed, the equations of motion are often simpler in a rotating frame than in an inertial one; this is definitely the case for orbits in Hill's problem, the stability of which, for the purpose of illustration, we now discuss in both rotating and nonrotating frames.

Numerical integrations of Hill's problem show that the largest stable retrograde orbits are nearly twice the size of the biggest prograde ones. This asymmetry is easily explained in a system centered on the asteroid and rotating at the asteroid's orbital angular velocity; the acceleration responsible is, of course, that of the eminent Monsieur Coriolis (HB1). Simple geometric considerations of the directions of $\mathbf{\Omega}$ and \mathbf{v}_{rot} show that the Coriolis acceleration has an outward component for prograde orbits and an inward component for retrograde ones; clearly an acceleration directed in this way diminishes the former's stability while enhancing the latter's. Let us consider this from a different perspective and recall that Hill's problem admits an integral of the motion which is obtained from conservation of total "energy" in the rotating frame; particle trajectories in phase space are therefore constrained to lie on

a surface of constant "energy." Although the Coriolis acceleration cannot push particles off this surface, it can still move them along the surface. Associated with the conservation of "energy" is a constraint in physical space that prevents a particle from crossing a zero-velocity curve. This restriction, however, does not stop the crafty M. Coriolis from pushing prograde particles up to the very edge of the ZVC while pulling retrograde ones away from it! In fact, when the ZVC is open to heliocentric space, M. Coriolis happily pushes prograde particles out through the neck of the curve and completely away from the asteroid; this is why the opening of the ZVCs is such a good indicator of escape for prograde orbits (HB1).

We can reach the same conclusions regarding the stability of prograde and retrograde orbits as viewed in a nonrotating frame whose origin remains on the asteroid; such a frame is of course noninertial owing to the acceleration of the coordinate system's origin. Here the difference in stability of the two orbital classes can be explained by the fact that their synodic periods differ. Recall that the *synodic period* is the time taken for a particle to return to the same orientation with respect to the Sun; this differs, in general, from the *sidereal period* which is the time taken for a particle to move to the same position relative to the "fixed" stars. In fact, prograde orbits all have synodic periods that are longer than their sidereal periods since, due to the asteroid's angular motion, prograde particles must travel a little further than one complete orbit to regain their original position with respect to the Sun. For retrograde orbits, the converse holds: sidereal periods exceed synodic ones. Escape from the asteroid, in both cases, occurs primarily along the Sun-asteroid line, either toward or away from the Sun where tidal effects are strongest (see Figs. 3, 10, and 11 of HB1). Because synodic periods for prograde orbits exceed those for equally sized retrograde ones, prograde orbits linger along the Sun-asteroid line, thereby allowing the destabilizing tidal force to build up greater orbital perturbations. We obtain the same result: prograde orbits are torn from the asteroid's gravitational grasp much sooner than their retrograde counterparts.

In the rest of this paper we shall adopt the rotating frame in our discussions of dynamics; one advantage of this choice is that the Coriolis acceleration neatly encapsulates all of the differences between prograde and retrograde orbits.

2. ECCENTRICITY EFFECTS

2.1. Analytic Treatment

2.1.1. Equation of motion. Our previous study of orbital stability summarized above assumes an asteroid on a circular orbit and although HB1 showed that an exact scaling law can connect results for asteroids with different

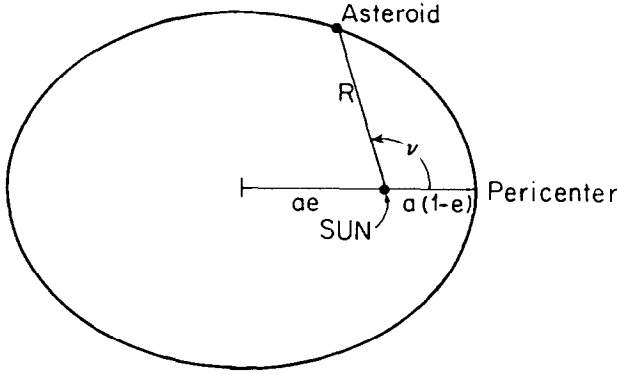


FIG. 1. An eccentric orbit showing the definitions of some of the variables used in the text. The Sun lies at one focus of the ellipse and the asteroid's true anomaly ν is the angle between the asteroid and pericenter as seen from the Sun. The instantaneous Sun-asteroid distance R is minimum at pericenter ($\nu = 0$) where it attains the value $a(1 - e)$.

masses and distances from the Sun, no such scaling to asteroids with other orbital eccentricities is expected to be possible. Since many asteroids and comets are on significantly elliptic orbits, this section explores the consequences of nonzero orbital eccentricity on the stability of circumasteroidal orbits.

An asteroid on an elliptic orbit moves around the Sun at a nonuniform angular rate which, written as a vector, is

$$\boldsymbol{\Omega} = \frac{d\nu}{dt} \hat{\mathbf{z}} = \left(\frac{GM_{\odot}}{R^3} \right)^{1/2} (1 + e \cos \nu)^{1/2} \hat{\mathbf{z}}, \quad (1)$$

where R is the instantaneous distance from the Sun given by

$$R = \frac{a(1 - e^2)}{1 + e \cos \nu}; \quad (2)$$

G is the gravitational constant; M_{\odot} is the solar mass; a , e , and ν are the asteroid's semimajor axis, eccentricity, and true anomaly, respectively; and $\hat{\mathbf{z}}$ is the unit vector normal to the asteroid's orbital plane (see Fig. 1). The true anomaly ν , which gives the angular location of the particle relative to pericenter, is a periodic function of time; thus $\boldsymbol{\Omega}$ and R also vary periodically. To study orbits in the vicinity of the asteroid, it is desirable to work in a coordinate system centered on the asteroid and rotating with it at the instantaneous angular velocity $\boldsymbol{\Omega}$ around the Sun, which is located along the negative x -axis. To first order in r/R , the equation of motion for a particle moving in such a frame can be shown to be

$$\frac{d^2 \mathbf{r}}{dt^2} = -\frac{GM_A}{r^2} \hat{\mathbf{r}} + \frac{GM_{\odot}}{R^3} [(3\mathbf{x} - \mathbf{z}) + e \cos \nu (\mathbf{x} + \mathbf{y}) + 2e \sin \nu (x\hat{\mathbf{y}} - y\hat{\mathbf{x}})] - 2\boldsymbol{\Omega} \times \mathbf{v}_{\text{rot}}. \quad (3)$$

Here $\mathbf{r} = r\hat{\mathbf{r}} = \mathbf{x} + \mathbf{y} + \mathbf{z}$ is the vector pointing from the asteroid to the particle, M_A is the mass of the asteroid, and \mathbf{v}_{rot} is the particle's velocity measured in the rotating frame. We omit "rot" subscripts on position coordinates since all positions in this paper are measured in the rotating frame. The velocity in the rotating frame is related to that in the nonrotating frame by

$$\mathbf{v}_{\text{rot}} = \mathbf{v} - (\boldsymbol{\Omega} \times \mathbf{r}), \quad (4)$$

where \mathbf{v} is the test particle's velocity relative to nonrotating coordinates; its magnitude for a circular orbit is simply $(GM_A/r)^{1/2}$. Taking $e = 0$ in Eq. (3), we recover Hill's equation (Eq. (2) in HBI). The three terms in Eq. (3) without explicit eccentricity dependence are the asteroid's gravitational attraction, the "tidal acceleration," and the Coriolis acceleration. These terms are discussed in greater detail by HBI and above; for our purposes here it suffices to note that the tidal term is outwardly directed for all orbits. The new terms are only present for nonzero eccentricity and so are dubbed the "eccentric" terms in the discussion below. The term with $e \cos \nu$ dependence is a correction to the centrifugal acceleration which arises from the difference in the asteroid's actual angular velocity from the angular velocity it would have if it were on a circular orbit at the same distance. Near pericenter, the asteroid's angular velocity exceeds that which it would have on a circular orbit (Eq. (1)) and hence there is an enhanced centrifugal acceleration away from the asteroid. Similarly, near the asteroid's apocenter, the angular velocity is significantly lower than it would be on a corresponding circular orbit; consequently the "eccentric centrifugal acceleration" is inwardly directed.

The term proportional to $e \sin \nu$ arises from the nonuniform rate of rotation of the reference frame; it vanishes at pericenter and apocenter where the angular acceleration (the time derivative of Eq. (1)) is zero. This acceleration always lies in the x - y plane and is tangent to a circle surrounding the asteroid. In contrast to the other accelerations discussed above, this acceleration can have a substantial component directed parallel or antiparallel to the particle's velocity; "energy" is added to the orbit in the former case and removed from it in the latter. Since the term has a $\sin \nu$ dependence, it causes "energy" to be added to retrograde orbits as the asteroid moves from apocenter to pericenter and removed during the return to apocenter. Prograde orbits lose "energy" as the asteroid drops toward pericenter but regain it over the second half of the cycle. For many orbits, there is little net change in the "energy" over the asteroid's complete orbital period. Nevertheless, acting over long times, we expect this acceleration to be destabilizing since it produces behavior analogous to a random walk in orbital "energy." Those orbits whose orbital "energy" is increased may eventually be driven to escape.

2.1.2. Hill sphere at pericenter scaling. In this section, our goal is to find a simple analytic way to extend results obtained for an asteroid with a given semimajor axis, eccentricity, and mass to a second asteroid with different values of these quantities. In Hill's problem when the asteroid's eccentricity was zero, HB1 found that such an extension was possible and that distances scale like the radius of the asteroid's Hill sphere $r_H = (\mu/3)^{1/3}a$, where $\mu \equiv M_A/M_\odot$ is the asteroid–Sun mass ratio. Thus, for example, if an interesting orbit were discovered to exist around one asteroid with zero eccentricity, an orbit with the *same shape* exists around all other asteroids which move on circular paths. This follows from the fact that Hill's problem in dimensionless form is parameter free.

These ideas extend readily to the case when the asteroid has nonzero eccentricity. To nondimensionalize Eq. (3), we choose to measure distances in units of the asteroid's Hill radius and angular velocities in units of the asteroid's mean motion $n \equiv (GM_\odot/a^3)^{1/2}$. With these choices and the definitions given in Eqs. (1) and (2), we can rewrite Eq. (3) as

$$\frac{d^2\mathbf{r}}{d\tau^2} = -\frac{3}{r^2}\hat{\mathbf{r}} + \left(\frac{1+e\cos\nu}{1-e^2}\right)^3 [(3\mathbf{x} - \mathbf{z}) + e\cos\nu(\mathbf{x} + \mathbf{y}) + 2e\sin\nu(x\hat{\mathbf{y}} - y\hat{\mathbf{x}})] - 2\frac{(1+e\cos\nu)^2}{(1-e^2)^{1.5}}(\hat{\mathbf{z}} \times \mathbf{v}) - 2\frac{(1+e\cos\nu)^4}{(1-e^2)^3}(\mathbf{x} + \mathbf{y}), \quad (5)$$

where $\tau = nt$ is the dimensionless time and \mathbf{v} is the particle's dimensionless velocity measured in the nonrotating frame. Since the only parameter in Eq. (5) is e (ν is a function of time), it follows that with a given eccentricity, the equations of motion are identical for asteroids of different sizes and distances from the Sun; changing these quantities only affects how we define the dimensionless units. In short, since distances are measured in Hill radii, our results scale with that distance. The more interesting question, however, is the following: How can we scale results from one asteroid to another when the two have different orbital eccentricities?

Clearly an exact scaling of results is impossible given the ν dependence of Eq. (5); accordingly we attempt to find an approximation valid for the orbits that we are most interested in, namely those that narrowly avoid escaping from the asteroid. Physical intuition and Eq. (5) show that the perturbation accelerations felt by a orbiting particle are maximum when the asteroid is near the pericenter of its orbit. In general, therefore, weakly bound particles have their closest brush with escape during the asteroid's pericenter passage and, given slightly more "energy," many of these particles would be expected to escape during this time. If we are only interested in determining what

will happen to the system in the short term (a few orbits of the asteroid around the Sun), and are only worried about marginal escapes, which occur near pericenter, then in some sense we can ignore what happens over the rest of the orbit. Taking $\nu = 0$ in Eq. (5), we claim that, apart from small differences in the centrifugal and Coriolis terms due to the faster angular velocity at pericenter, the result is just the equation of motion for orbits around an asteroid with $e' = 0$ and $a' = a(1 - e)$. In other words, for the purposes of studying marginal escapes on short time scales, an asteroid moving through its pericenter can be reasonably well approximated by a second asteroid moving on a circular orbit at the pericenter distance of the first. A similar tack is taken by Lecar *et al.* (1992) in quite a different context.

In order to justify this claim, we must show that the perturbation accelerations arising from the asteroid's faster angular velocity at pericenter are small compared to the perturbations due to the asteroid's closer distance to the Sun. Consider first the second term on the right side of Eq. (5) which, evaluated at pericenter ($\nu = 0$), becomes

$$\mathbf{a}_{\text{tidal}} = \frac{[3\mathbf{x} - \mathbf{z} + e(\mathbf{x} + \mathbf{y})]}{(1-e)^3}. \quad (6)$$

Expanding Eq. (6) in a Taylor series in e , we find the first-order term is given by

$$e[9\mathbf{x} - 3\mathbf{z}] + e[\mathbf{x} + \mathbf{y}], \quad (7)$$

where the first term in brackets arises from the asteroid's closer distance to the Sun and the second comes from the increased angular velocity. The distance terms are significantly larger, especially for particles along the x -axis where escape invariably occurs. This remains true for higher-order terms in the Taylor expansion although the magnitude of the difference decreases somewhat. Treating the Coriolis acceleration in the same manner, we find that at pericenter it can be written in the form

$$\mathbf{a}_{\text{Coriolis}} = -2\frac{[1+e]^{1/2}}{[1-e]^{3/2}}(\hat{\mathbf{z}} \times \mathbf{v}_{\text{rot}}) - 2\frac{[1+e]}{[1-e]^3}(\mathbf{x} + \mathbf{y}); \quad (8)$$

here the terms in the denominators arise from the asteroid's closer distance to the Sun while those in the numerators are due to the variation of the asteroid's velocity along its elliptic path. As before, we find the change in distance is the dominant effect, accounting for $\geq 75\%$ of the variance in the Coriolis acceleration for all values of the eccentricity.

Since the terms arising from the asteroid's increased angular velocity at pericenter are small compared to the

terms owing to its location closer to the Sun, we can—as a first approximation—ignore the velocity terms. A particle’s equation of motion around an asteroid near pericenter is then identical to the equation of motion of a particle around a second asteroid on a circular orbit at the pericenter distance of the first. Furthermore, since the stability of weakly bound orbits is put to the greatest test during the asteroid’s pericenter passage, the most important factor determining escape is clearly how closely the asteroid approaches the Sun. The synthesis of these results suggests that the size of the asteroid’s stability zone is simply proportional to the asteroid’s pericenter distance. Combined with HB1’s previous result for an asteroid on a circular orbit, we have that *the size of an asteroid’s stability zone is roughly proportional to the size of the Hill sphere calculated at the asteroid’s pericenter* i.e. $r_{\text{HP}} \approx (\mu/3)^{1/3} a(1 - e)$.

This is a very strong assertion. It states that, if we can ascertain the size of the stability zone for one asteroid, we can estimate it for other asteroids with different masses, semimajor axes, and eccentricities. As noted above and in HB1, scaling to an asteroid with a different semimajor axis is mathematically exact and scaling to an asteroid with a different mass only errs to the order of the asteroid–Sun mass ratio which is entirely negligible. Thus any given orbit around one asteroid has a counterpart around another asteroid with an *identical shape* if the orbital eccentricities of the two asteroids are the same. Since the stability surface is composed of multiple orbits all of which scale in this way, it does too. We have now shown that for orbits of short duration around asteroids with different eccentricities, most (perhaps 70–80%) of the effects of eccentricity on the size of the stability surface can be accounted for by scaling the surface as the Hill sphere calculated at the asteroid’s pericenter. In the sections to follow, we use the $e = 0$ results from HB1 to make predictions for asteroids with nonzero eccentricity and then compare these predictions with actual numerical integrations. We also discuss the validity of the approximations made for three representative cases: prograde, retrograde, and $i = 90^\circ$ orbits.

2.1.3. The Jacobi integral. First, however, we digress slightly and consider the Jacobi integral which, after all, is one of the most powerful results available for the circular restricted problem of three bodies. In the circular case, the Jacobi integral allows the derivation of zero-velocity surfaces which place simple, but often useful, restrictions on the portion of space accessible to particles starting with given initial conditions. HB1 applied these surfaces to an asteroid on a circular orbit; here we examine the difficulties inherent in extending this analysis to asteroids on eccentric orbits.

Attempting to obtain the Jacobi integral in the standard

way, we first take the scalar product of Eq. (3) with \mathbf{v}_{rot} to obtain

$$\mathbf{v}_{\text{rot}} \cdot \dot{\mathbf{v}}_{\text{rot}} + \frac{GM_A}{r^2} \dot{r} = \frac{GM_\odot}{R^3} [(3x\dot{x} - z\dot{z}) + e \cos \nu(x\dot{x} + y\dot{y}) + 2e \sin \nu(xy\dot{x} - y\dot{x})], \quad (9)$$

where the Coriolis term has vanished since it is perpendicular to \mathbf{v}_{rot} . The next step is to integrate Eq. (9) over time. The terms on the left are directly integrable, but those on the right, especially the last one, are more stubborn. These right-hand terms are implicit functions of time through both the particle’s coordinates and the asteroid’s true anomaly, and hence they cannot be integrated for an unknown orbit. Thus we find a Catch-22: although a Jacobi integral exists for the case where the primary’s orbit along ellipses, it is not known how to express the integral in a useful manner (Szebehely and Giacaglia 1964). That is to say, to obtain useful information from the Jacobi integral, the trajectory of the particle must be known but knowledge of the particle’s trajectory makes the information contained in the integral redundant!

Once again, because we are mainly interested in orbits during the asteroid’s pericenter passage, we look for a result that can be applied in that region. Taking $\nu = 0$ in Eq. (9) eliminates the final term and allows the time integration to be performed. Carrying out the integration and switching to slightly different dimensionless units ($GM_\odot/r_p^3 \equiv 1$, $(\mu/3)^{1/3}r_p \equiv 1$, where $r_p = a(1 - e)$ is the pericenter distance), we obtain

$$C = \frac{6}{r} + 3x^2 - z^2 + e(x^2 + y^2) - v_{\text{rot}}^2. \quad (10)$$

This equation with $v_{\text{rot}} = 0$ determines the shape of the ZVCs instantaneously at the asteroid’s pericenter. The application of Eq. (10) is approximate, and even then strictly limited to a small time Δt near a single passage of an asteroid through pericenter; similar conclusions are reached through more rigorous derivations (Szebehely and Giacaglia 1964, Ovenden and Roy 1961). If one attempts to apply Eq. (10) to two successive pericenter passages, unmodeled effects such as the final term in Eq. (9) acting in the interim might alter C , the Jacobi “constant.” Fortunately, such modifications are usually small for short time periods, and we can normally apply Eq. (10) to orbits followed for a few pericenter passages of the asteroid.

Comparing Eq. (10) to the equivalent expression for a circular orbit we find that the two differ only by the excess centrifugal potential $e(x^2 + y^2)$. As an illustration of the slight difference, we calculate the locations where the zero-velocity surfaces surrounding the asteroid first open

up. These positions occur at saddle points of Eq. (10) (with $v_{\text{rot}} = 0$) which are also equilibrium points of Eq. (3) (with $\nu = 0$). Setting the partial derivatives of Eq. (10) equal to zero, we find that the openings of the ZVCs occur at the points ($x = \pm x_{\text{crit}}$, $y = 0$, $z = 0$), where x_{crit} and the corresponding Jacobi “constant” are given by

$$x_{\text{crit}} = \left(\frac{3}{3+e} \right)^{1/3}; \quad C_{\text{crit}} = \frac{9}{x_{\text{crit}}}. \quad (11)$$

As the eccentricity is increased in Eq. (11), the opening of the zero-velocity surfaces occurs closer to the asteroid; this can be qualitatively understood by noting that the equilibrium points occur nearer the asteroid as a result of the additional outwardly directed centrifugal acceleration at pericenter. For $e = 0$, we recover the more familiar results $x_{\text{crit}} = 1$ and $C_{\text{crit}} = 9$ (see HB1, Chauvineau and Mignard 1990a); while, conversely, taking the extreme case $e = 1$, we obtain $x_{\text{crit}} \approx 0.91$ and $C_{\text{crit}} \approx 9.9$, differences of only $\sim 10\%$. We conclude, as above, that the influence of the additional centrifugal acceleration is minimal.

2.2. Integrations

2.2.1. General. Now that some intuition has been developed about the effect of the asteroid’s orbital eccentricity, we present the results of our numerical integrations. For comparison purposes, we take the particle to have the same initial conditions used by HB1 and discussed in Section 1.1 above; furthermore we set the asteroid’s semimajor axis to 2.55 AU in all of our integrations. The addition of orbital eccentricity, however, complicates matters by requiring the specification of two extra items, namely the eccentricity of the orbit and the asteroid’s position along its orbit at the time the particle is launched. The second of these complications has lesser significance since we follow the test particle’s motion during the time it takes the asteroid to complete five orbits around the Sun (≈ 20 years); thus usually the influence of different starting positions should be minimal. For simplicity, therefore, we choose to start the asteroid at the apocenter of its heliocentric orbit in all of the following integrations. This choice should provide a stringent test of our neglect of the “eccentric” terms in the above discussion since these terms are allowed to act for some time before escape, which generally occurs during the pericenter passage, is possible. Even with this reduction of the problem, a thorough exploration of the three-dimensional phase space (asteroid’s eccentricity, particle’s inclination, particle’s starting distance) would require approximately $(10 \text{ eccentricities}) \times (20 \text{ inclinations}) \times (25 \text{ starting distances}) = 5000$ initial conditions. To reduce this to a more manageable number we take four two-dimensional slices

through this phase space, three at constant inclinations representing the three classes of orbits discovered to be important in HB1 (prograde, retrograde, and highly inclined), and one at the measured eccentricity of the asteroid Gaspra. Table I lists relevant asteroid parameters.

2.2.2. Prograde orbits. Prograde orbits provide the best test of the ideas presented above since, at least in the circular case, particles on such orbits usually escape very quickly whenever their ZVCs are open (HB1). We might be tempted, therefore, to predict that escapes will occur when the ZVC evaluated at the asteroid’s pericenter is open, but before we can confidently make such a prediction, an additional factor must be considered. Imagine that escape is energetically possible as the asteroid nears pericenter, but the particle is located at a disadvantageous spot for escape to occur, say 90° away from the Sun–asteroid line. Then to give the particle a fair chance to escape, we must either require that the asteroid remain near pericenter long enough for the grain to complete a reasonable fraction of one orbit around the asteroid or, equivalently, we must integrate through multiple pericenter passages so that many opportunities to escape arise, some of which will find the particle in a favorable position. The prograde orbits with the longest periods are those near the limits of stability; these have synodic periods that are about $1/4$ of the asteroid’s period if the minor planet is on a circular orbit. For an eccentric asteroid orbit with the same semimajor axis, the stability zone is smaller and the particles orbit even faster. Thus we expect that five pericenter passages of the asteroid about the Sun should usually allow the particle ample opportunity to escape.

Figure 2 shows the results of nearly two hundred orbital integrations carried out for initially circular prograde orbits at a variety of distances from asteroids with differing eccentricities. We treat the full range of possible eccentricities; the low-to-moderate values are generally applicable to asteroids, while the larger are more appropriate for comets. The boundary line extends the critical distance found in HB1 to asteroids with nonzero orbital eccentricity using the scaling result of Section 2.1.2. The division plots as a straight line in the (e, R_A) coordinates used in Fig. 2 because the critical distance, like the size of the stability zone, is proportional to the asteroid’s pericenter distance $a(1 - e)$. For these prograde orbits, the line also selects the initial condition corresponding to the critical pericenter ZVC (ignoring the small eccentricity dependence discussed in Section 2.1.3). Thus only particles with initial conditions above the line have ZVCs that are instantaneously open near pericenter. It is apparent that no orbits below the line escape; note, however, that this trapping is not necessarily required by the argument of closed ZVCs because accelerations that were ignored in developing these ZVCs can cause orbits to cross them.

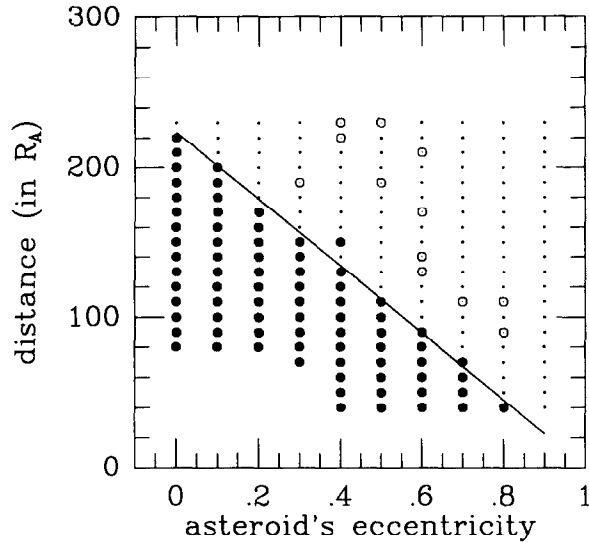


FIG. 2. The orbital fate of nearly 200 particles on *prograde* orbits around an asteroid at 2.55 AU. Each particle was given the velocity that would put it on an initially circular path around the minor planet. A solid circle signifies a particle that remains in the asteroid's vicinity for at least 20 years, a small dot corresponds to a grain that escapes into heliocentric space, while an open circle with a dot inside represents a particle that strikes the asteroid's surface. The diagonal line is the predicted division between bound and escape orbits; its derivation is based on scaling the Hill sphere at pericenter as developed in the text.

Nevertheless, as we argued above, these accelerations should be small, so the fact that no escapes are seen to occur from below the boundary is encouraging. Furthermore, there is only a single bound orbit that lies significantly above the division. This lone particle was never in the right place to get a boost from M. Coriolis at pericenter; it would almost certainly escape with increased integration time.

The distribution of orbits that strike the asteroid in Fig. 2 displays an interesting regularity. All of these crash orbits are found above the division line at which particles become unbound. The lack of crash orbits below the line is consistent with the character of bound prograde and retrograde orbits which are usually very regular in appearance and rarely display chaotic behavior (cf. Chauvineau and Mignard 1990a). As we will see presently, however, the separation of bound and crash orbits observed here for prograde orbits is not a result that can be extended to three-dimensional paths.

2.2.3. Inclined orbits. Bound orbits with inclinations in the range $60^\circ < i < 120^\circ$ have many similar characteristics (HB1); accordingly we choose $i = 90^\circ$ orbits as typical examples of this class. The largest of these orbits is comparable to the largest of the prograde orbits, so the maximum period for bound, inclined orbits is also about 1/4 of an asteroid period. By the argument advanced above, five

pericenter passages of the asteroid about the Sun should be enough to allow most particles that are destined to escape to be dislodged. But HB1 find that the opening of the ZVCs is not a good indicator of escape for orbits with $i \geq 30^\circ$ since the Coriolis acceleration for these orbits does not have the large radially outward component characteristic of that for prograde orbits. We therefore discontinue our use of critical ZVCs as an escape criterion, instead focusing on Hill sphere scaling as described in Section 2.1.2 to connect our results for an asteroid on a circular orbit to those with nonzero eccentricity.

The line in Fig. 3 shows the application of this scaling. It does remarkably well, although not nearly as well as in the prograde case. The reason for this is clear. A prograde orbit will almost always escape if the corresponding ZVC is open, and will rarely escape if the ZVC is closed (recall that for eccentrically orbiting asteroids the ZVC is just an approximation); this idea is reflected in the sharpness of the empirical boundary seen in Fig. 2. Inclined orbits, on the other hand, are not so strictly constrained. Many remain at least temporarily in the asteroid's vicinity even if their ZVCs are wide open; hence the division between bound and unbound inclined orbits is "fuzzier" than the division in the prograde case. Several bound orbits are located in the region dominated by escape orbits and a few escape orbits are even found below the line in the region where this criterion asserts that orbits should be bound. Note also that crash orbits are inextricably interwoven with both bound and escape paths. This result is consistent with a similar one for the circular case (HB1) where many crash orbits are found in the vicinity of the

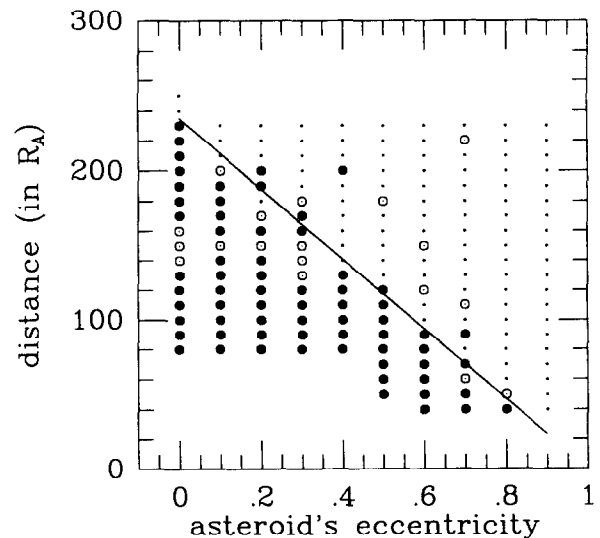


FIG. 3. Same as Fig. 2 for initially circular orbits with *inclination* $i = 90^\circ$. As in Fig. 2, the approximate theoretical division separating bound and escape orbits matches the data quite impressively; the decrease of stability with increasing eccentricity is very evident.

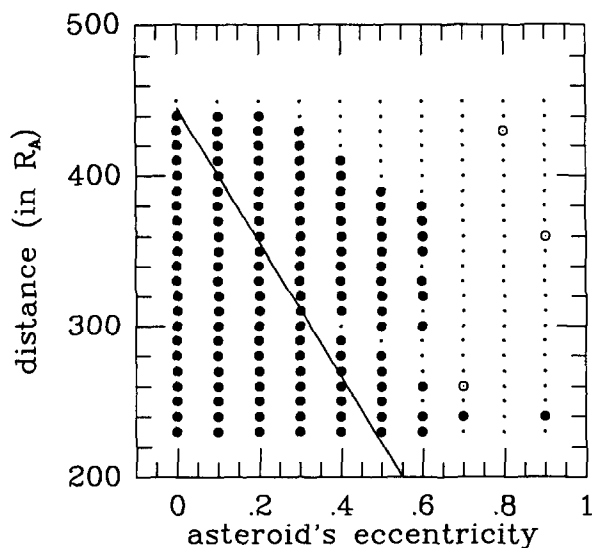


FIG. 4. Same as Fig. 2 for initially circular *retrograde* orbits. Note the sparsity of orbits that strike the asteroid. For retrograde orbits, the calculated bound–escape division disagrees with the data for reasons that are discussed in the text (compare Figs. 2 and 3).

critical distance. The ubiquity of crash orbits in these circumstances is a direct consequence of the dynamics of such orbits as HB1 discuss in some detail.

2.2.4. Retrograde orbits. The situation for retrograde paths about elliptically orbiting asteroids is not as good as for the two cases discussed above for several reasons. First, since bound retrograde orbits are relatively large, their periods are about four times the period of biggest prograde orbits; this implies that integrations of five asteroid years may not be sufficiently long to explore the full dynamical range. In addition, since these orbits are about twice the size of the ones considered previously, the asteroid's gravity is much weaker and the perturbations are significantly larger (see Fig. 3 of HB1). Consequently the unmodeled parts of these forces are more important for retrograde orbits than for either prograde or inclined ones. As an example, the Coriolis acceleration pulls more strongly inward at the asteroid's pericenter for retrograde orbits than simple scaling would suggest and this augments the stability of these orbits around asteroids on eccentric paths. Finally the point at which the ZVCs first open for retrograde orbits is only about 25% of the distance to where escapes first occur assuming an asteroid on a circular orbit. The constraint provided by the retrograde ZVCs, therefore, is almost useless (cf. HB1, Chauvineau and Mignard 1990a).

Figure 4 shows our results for planar retrograde orbits. The scaling law that worked so well for the prograde and inclined orbits clearly fails here: many bound orbits are found above the line where the theory predicts only es-

cape orbits. The behavior is not even linear; note the abrupt drop in stability that occurs for an asteroid eccentricity of 0.7. This steep falloff suggests that longer integrations would lead to additional escapes, at least near this edge. Furthermore, the finger of escape orbits extending into the bound orbits at a distance of about 300 asteroid radii also hints that the bound orbits above the finger will escape given a few more pericenter passages. But increasing the integration time will not solve all of the problems encountered here. We recall the results of Zhang and Innanen (1988), who, after tracking orbits for 1000 years, found that the critical distances for initially circular retrograde orbits around asteroids with eccentricities of 0.0 and 0.07 were 445 and 358 R_A , respectively. The $e = 0$ result agrees with our finding for a 20-year integration; thus, scaling to the pericenter of an $e = 0.07$ orbit (see Fig. 4), we would predict a critical distance of 410 R_A , or about 15% larger than the numerical result. Evidently the analysis of these retrograde orbits is hampered by both insufficient integration times and inadequate approximations.

2.2.5. "Gaspra" ($e = 0.17$). As a final test and an independent verification of the ideas addressed above, and because of the destination of a certain spacecraft, we carried out a more thorough investigation of the stability of orbits about an idealization of the asteroid 951 Gaspra. The results are displayed in Figs. 5 through 7. The first of

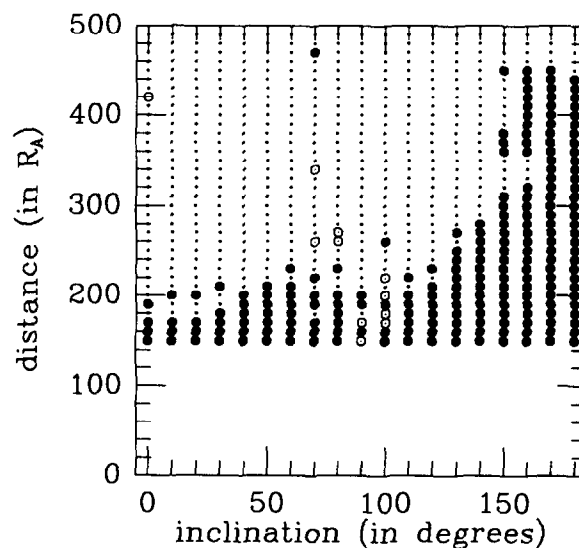


FIG. 5. The fate of about 650 particles started at different inclinations for an asteroid on an orbit with semimajor axis $a = 2.55$ AU and an eccentricity $e = 0.17$. Note the prevalence of impacts for orbits with inclinations near 90° . We can scale this plot for application to "Gaspra" ($a = 2.2$ AU and $e = 0.17$): since the eccentricities of the two asteroids are identical, and differences in their masses are accounted for by measuring distances in R_A , the abscissa need only be multiplied by the ratio of the two semimajor axes, namely $2.20/2.55 \approx 0.86$.

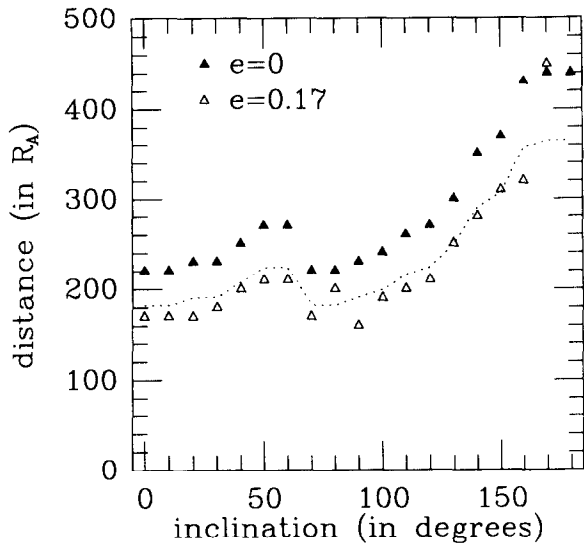


FIG. 6. Maximum starting distance for those initially circular orbits that remained bound to the asteroid (for about 20 years) as a function of the orbiting particle's initial inclination. Data are plotted for two values of the asteroid's orbital eccentricity, $e = 0$ and $e = 0.17$; in both cases $a = 2.55$ AU. The dotted line is the prediction for $e = 0.17$ derived from scaling the $e = 0$ result with the Hill sphere at pericenter. In this case the two semimajor axes are identical, so scaling is accomplished by simply multiplying the $e = 0$ results by $1 - 0.17 = 0.83$. The plot clearly shows the erosion of the zone of stability caused by increasing the asteroid's orbital eccentricity.

these shows the fate of particles as a function of their starting distance and initial inclination for an asteroid with Gaspra's eccentricity of 0.17 (cf. HB1, Fig. 15 which has $e = 0$). Note that these integrations are for an object at 2.55 AU; for application to "Gaspra," which orbits at 2.2 AU, distances need to be reduced by a numerical factor equal to the ratio of the respective Hill sphere radii. For distances measured in R_A , as are the abscissas in Figs. 5 through 7, this factor is simply the ratio of the semimajor axes of the two asteroids.

We estimate the critical distance from Fig. 5 by taking, for each inclination column, the outermost bound orbit such that there are no escape orbits below it; this procedure eliminates freak orbits such as the one at ($i = 70^\circ$, $d = 470 R_A$). The results, critical distance as a function of inclination, are plotted in Fig. 6 along with similar results for an asteroid with $e = 0$ (from Fig. 15 of HB1). The dotted line in Fig. 6 is the expected result for $e = 0.17$ which has been scaled from the $e = 0$ data; comparing the predictions to the actual integrations, we see that prograde and inclined orbits actually escape at distances slightly less than predicted, but well within expected errors arising from the neglected effects. In those regions of Fig. 5 where there are many crash orbits, the division

between bound and escape orbits is poorly constrained; this leads to a "choppiness" in the critical distance which is observed in the $e = 0.17$ data near $i = 90^\circ$ in Fig. 6. Unlike prograde and inclined orbits, retrograde ones exhibit little loss of stability; once again suspicion falls on insufficient integration times.

To describe the volume in which bound material might be present about asteroids on circular heliocentric orbits, HB1 used the "stability surface." They noted that its typical radius up to latitudes of 35° was nearly constant and was significantly larger than its vertical dimension which was approximately constant for latitudes greater than 35° (i.e., its shape is like a sphere with the poles sliced off). Because polar orbits are less stable than retrograde ones for asteroids on elliptic orbits as well as those on circular paths (Fig. 6), we anticipate a similar morphology for the stability surface in the current case. Figure 7 plots the largest out-of-plane distance (z -coordinate) from the union of all orbits with a given starting inclination that lie within the critical distance; for comparison, we also plot results for a circular asteroid orbit. We see that the maximum height to which material around Gaspra can rise is only about 75% the value it would have above an asteroid on a circular orbit. The dotted line in Fig. 7, the prediction of direct Hill sphere scaling of results for $e = 0$, suggests that the value should be 83%. Clearly the correlation between the dotted line and the $e = 0.17$ data is worse in Fig. 7 than it is in Fig. 6; this difference reflects

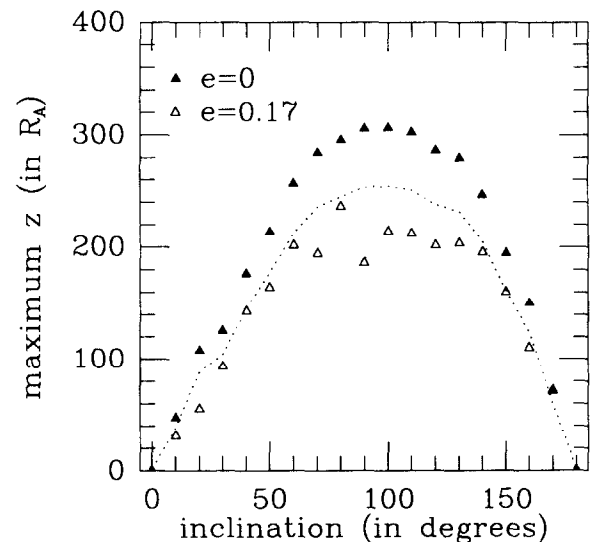


FIG. 7. Maximum height above the asteroid's orbital plane attained by the particles from Fig. 6; as in that figure, the dotted line is the prediction for the lower set of data obtained by scaling from the upper set. The data displayed here show that as the asteroid's eccentricity is increased, orbits that rise to large heights above the orbital plane disappear faster than our simple scaling would suggest.

changes in the orbital evolution of the inclined orbits under accelerations ignored in our analysis.

These numerical experiments indicate that bound debris should not be present beyond about $200 R_A$ above Gaspra's orbital pole. We remind the reader that our study has dealt only with the question of which orbits are stable and which are unstable. To actually estimate the probability that a spacecraft might strike something would require a knowledge of the population mechanisms for circum-asteroidal orbits. Most discussions of debris sources (Weidenschilling *et al.* 1989, Burns and Hamilton 1992) favor the likelihood that circumasteroidal debris, if any exists at all, will be produced much closer to the minor planet than the distant orbits considered here. Thus our criterion is likely to be quite conservative; that is, a spacecraft should be able to safely pass much closer to the asteroid than the distance quoted above.

3. RADIATION PRESSURE

All objects in interplanetary space are subject to perturbations not only from the gravitational attractions of the planets, but also from the absorption and subsequent re-emission of solar photons and corpuscular radiation. Of the many forces (radiation pressure, Poynting–Robertson drag, Yarkovsky effect, etc.; see the review by Burns *et al.* (1979)) that arise from this process, radiation pressure is by far the strongest. Radiation pressure arises primarily from the absorption of the momentum of solar photons and consequently is directed radially outward from the Sun. The force's strength is proportional to the solar flux density which has the same inverse square radial dependence as the Sun's gravity; hence radiation pressure is usually written as a dimensionless quantity β times solar gravity. For spherical particles that obey geometrical optics,

$$\beta = 5.7 \times 10^{-5} \frac{Q_{pr}}{\rho s}, \quad (12)$$

where s and ρ are the particle's radius and density in cgs units and Q_{pr} is a constant whose value depends on the optical properties of the grain (Burns *et al.* 1979). This result applies to particles larger than about a half-micrometer, the wavelength of a photon at the peak of the solar spectrum. When a particle's characteristic size is similar to the wavelength of incident light, Mie scattering occurs, Q_{pr} is no longer constant, and β becomes a complex function of particle size. In contradiction to Eq. (12), which predicts that the strength of radiation pressure will increase for smaller particles, it actually decreases (Burns *et al.* 1979) because most solar photons are in the visible and such photons interact only weakly with very small

grains. In the rest of this work, we confine ourselves to large grains which obey Eq. (12).

3.1. Heliocentric vs Circumplanetary Orbits

The acceleration of a particle on a heliocentric orbit is determined by the sum of the inward force of solar gravity and the outward force of radiation pressure, which can be combined into a single $1/r^2$ force with magnitude $(1 - \beta)$ times solar gravity. The grain's orbital dynamics is then identical to the gravitational two-body problem with a reduced solar mass; if a particle's size, and hence its β , is constant, its orbit will be a conic section. Only if the particle's β changes abruptly, as when a small grain is ejected from a comet, or gradually, as in the case of a subliming grain, will its orbital evolution be nontrivial (Burns *et al.* 1979). Radiation pressure, therefore, does not significantly alter the nature of most heliocentric orbits and, accordingly, it has received scant attention in the literature.

The situation is quite different for particles that orbit a planet rather than the Sun (Milani *et al.* 1987); since the planet itself is essentially uninfluenced by radiation pressure while small objects orbiting it may be, the problem cannot be treated by simply reducing the mass of the Sun as in the case of heliocentric orbits. Furthermore, the dominant forces are different in each problem; in the case at hand, the important forces are the asteroids gravity and the solar tidal force rather than direct solar gravity as in the heliocentric problem. In many cases, therefore, radiation pressure produces stronger effects on circumplanetary orbits than on solar orbits; we show the truth of this statement when the "planet" is actually a large asteroid with a radius of 100 km.

Since radiation pressure typically induces much smaller accelerations than the asteroid's gravity, an orbit-averaged perturbation technique is often appropriate. This analysis, leading to a simplified set of differential equations describing the evolution of the osculating orbital elements due to an external force which is constant in magnitude and direction, has been carried out by Burns *et al.* (1979) and Chamberlain (1979), among others. The semimajor axis of a circumplanetary orbit is found to be unchanged by radiation pressure. Burns *et al.* solved the planar system ($i = 0$) considering small eccentricity and weak radiation pressure, assumptions applicable to most situations arising in the Solar System. Their solution was later extended to arbitrary eccentricities and moderate radiation pressure by Mignard (1982). Both Burns *et al.* and Mignard find periodic oscillations in the orbital eccentricity that, for weak radiation pressure, vary with the planet's orbital period. The solution to the full system with arbitrary inclination, as derived by Mignard and Hénon

(1984), involves complicated coordinate transformations that render the study of an orbit with initial conditions expressed in orbital elements impractical. The planar solution shows, however, that if radiation pressure is sufficiently strong, it can induce eccentricities large enough that particles are forced to crash into the asteroid (cf. Peale 1966). This mechanism, which provides the potential to efficiently remove tightly bound material from circumasteroidal orbits, is discussed further in the sections to follow.

3.2. Zero-Velocity Curves

As we noted in Section 2.1.3 above, the existence of the Jacobi integral and its associated zero-velocity curves proves to be useful in addressing the eventual fate of loosely bound, prograde orbits. Accordingly, in this section we explore zero-velocity curves derived with the inclusion of solar radiation pressure; as a first approach to the problem and to avoid the difficulties encountered above, we treat only the case of circular asteroid orbits. For circular orbits, we find that exact results exist; extending the results to eccentrically orbiting asteroids, however, entails the same approximations discussed in Section 2.1.3.

The existence of a Jacobi integral for the restricted three-body problem with radiation pressure is anticipated since radiation pressure in the rotating frame can be derived from a time-independent potential. Indeed, the addition of radiation pressure to solar gravity does not greatly complicate the problem since these forces are identical in both direction and radial dependence. In fact, the derivation of the Jacobi integral and the zero-velocity curves in the photogravitational, restricted, circular three-body problem proceeds along almost identical lines as the "classical" derivation (Schuerman 1980). Extensive analysis of the stability of the resulting equilibrium points has been carried out by Luk'yanov (1984, 1986, 1988). We now apply these ideas to Hill's problem, which, like the restricted problem, has an integral of the motion.

Incorporating radiation pressure into the equation of motion (Eq. (3) with $e = 0$), we obtain

$$\frac{d^2 \mathbf{r}}{dt^2} = -\frac{GM_A}{r^2} \hat{\mathbf{r}} + \frac{GM_\odot}{a^3} [3\mathbf{x} - \mathbf{z}] - 2\boldsymbol{\Omega} \times \mathbf{v}_{\text{rot}} + \beta \frac{GM_\odot}{a^2} \hat{\mathbf{x}}, \quad (13)$$

where we have taken incoming solar rays to be parallel, an assumption that is valid in the vicinity of our asteroid. Assuming β is time-independent, the final acceleration on the right-hand side of Eq. (13) can be integrated to give the potential $\beta(GM_\odot/a^2)x$. Taking the scalar product of

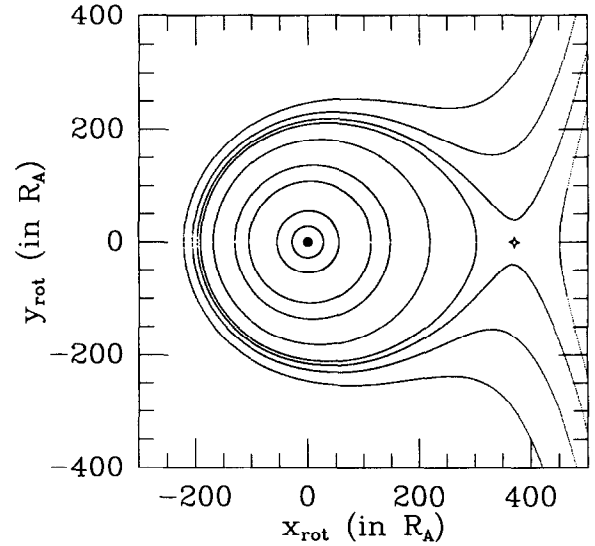


FIG. 8. Zero-velocity curves, including solar radiation, for a 1-mm particle around "Amphitrite." The Sun is located far out along the negative x -axis and the asteroid is the solid circle (not drawn to scale) at $(0, 0)$. Associated with each curve is a unique value of the Jacobi constant; larger curves have smaller Jacobi constants. The four-pointed star, located at $(370, 0)$, denotes the equilibrium point where all forces balance for 1-mm particles; a second equilibrium point lies between the asteroid and the Sun at $(-579, 0)$.

Eq. (13) with \mathbf{v}_{rot} , integrating over time, and nondimensionalizing, we find

$$C = \frac{6}{r} + 3x^2 - z^2 + 2\beta \left(\frac{3}{\mu}\right)^{1/3} x - v_{\text{rot}}^2. \quad (14)$$

Equation (14) depends on the parameter $\beta\mu^{-1/3}$ and so, as in the case of nonzero orbital eccentricity, care must be exercised when scaling from one asteroid to another. In particular, results scale as the Hill sphere only if the parameter $\beta\mu^{-1/3}$ is kept constant. This can be shown more explicitly by examining Eq. (13) in the same manner that we studied Eq. (3) in Section 2.1.2. If Q_{pr} and the particle and asteroid mass densities are constant, then β is inversely proportional to the particle's radius s (Eq. (12)) and $\mu^{-1/3}$ is inversely proportional to the asteroid's radius R_A . Thus, simply stated, results from a small asteroid can be applied to a larger one if the product of the asteroid's radius and the radius of the orbiting particle is kept constant.

We can derive zero-velocity curves from Eq. (14) by setting $v_{\text{rot}} = 0$ and choosing a particular value of C . For weak radiation pressure, the shape of the resulting zero-velocity curves differs only slightly from the more familiar ZVCs of Hill's problem; for stronger radiation pressure, however, the difference is marked. In an attempt to pro-

vide the reader with some insight into the constraints on escape imposed by the ZVCs, we discuss their shape for a moderate value of radiation pressure, namely that appropriate for 1-mm particles around ‘‘Amphitrite.’’ Several ZVCs are drawn in Fig. 8; these are simply plots of Eq. (14) with $v_{\text{rot}} = 0$ and $z = 0$ for different values of the Jacobi constant C . The small circles that closely surround the asteroid have large Jacobi constants; their shape is primarily determined by the asteroid’s gravity (cf. discussion by Chauvineau and Mignard (1990a) for ZVCs without radiation pressure). As C is decreased, the circles grow larger and begin to distort due to the tidal and radiation-induced accelerations. Because they both are directed along the x -axis, these perturbation accelerations cause a distortion of the ZVCs along that axis. The tidal potential is an even function of x and thus causes an elongation symmetric about $x = 0$ (see HB1, Figs. 5 and 10). In contrast, radiation pressure, because it always acts in the \hat{x} -direction, causes a nonsymmetric distortion, shifting the ZVCs away from the Sun. We see that radiation pressure is dominant for 1-mm particles since the outer curves of Fig. 8 are highly asymmetric. One consequence of this asymmetry is that as the Jacobi constant is decreased, the curves open away from the sun before they open toward it. Radiation pressure allows sufficiently energetic particles to escape in the antisunward direction; escape in the sunward direction, which requires still more ‘‘energy,’’ occurs more rarely.

When discussing Fig. 8, we carefully avoided quoting any actual numbers for the Jacobi constants or the location of the point at which the ZVCs open (see, however, the figure caption). This was done to keep the discussion general and therefore applicable to a large range of radiation pressure strengths. In reality, the Jacobi constant and the points where the ZVCs open are all functions of the relative strength of radiation pressure. To solve for the opening positions, which occur at the equilibrium points of Eq. (13), we set the partial derivatives of Eq. (14) (with $v_{\text{rot}} = 0$) equal to zero (cf. Danby 1988, p. 260). Thus, defining

$$\gamma = \frac{\beta}{3} \left(\frac{3}{\mu} \right)^{1/3}, \quad (15)$$

we find two solutions which lie on the x -axis ($y = z = 0$) at positions given by solutions to the cubic

$$x^3 + \gamma x^2 \mp 1 = 0, \quad (16)$$

where the upper sign refers to the critical point furthest from the Sun and the lower sign to the one closest to the Sun. Solving Eq. (16) for $\gamma \lesssim 1$ (weak-to-moderate radiation pressure), we obtain $x_{\text{crit}} \approx \pm(1 \mp \gamma/3 + \gamma^2/9)$

and $C_{\text{crit}} \approx 9 \pm 6\gamma - \gamma^2$. We find that there are indeed two critical ZVCs, since the two opening points occur at different values of the Jacobi constant. Thus if more curves with ever-decreasing Jacobi constants were plotted in Fig. 8, we would eventually see a tunnel from the asteroid to heliocentric space opening up on the left side of the figure. For $\gamma \gg 1$ and $x_{\text{crit}} > 0$, we find $x_{\text{crit}} \approx \gamma^{-1/2}$, which tends toward zero, and $C_{\text{crit}} \approx 12\gamma^{1/2}$.

3.3. Integrations

Our philosophy in adding the effects of eccentricity and radiation pressure to the escape problem is to separate the two so that a more direct comparison with the results of HB1 is possible. Accordingly, in all subsequent numerical integrations, we place the asteroid on a circular orbit around the Sun. As before, we model the asteroid 29 Amphitrite with the parameters given in Table I. We start particles out along the x -axis away from the Sun with a speed such that the orbit would be circular in the absence of all perturbations. As in the first half of this paper, we allow the velocity vector to take on one of three inclinations relative to the orbital plane: prograde ($i = 0^\circ$), retrograde ($i = 180^\circ$), or inclined ($i = 90^\circ$). As discussed above, these inclinations are representative of the three basic classes of circumasteroidal orbits in the case when radiation pressure is absent (HB1). The period of integration was set at five asteroid years (≈ 20 years) to facilitate comparison with our previous results.

Although these are the same initial conditions used in HB1 and in the case of an eccentric orbit above, they are particularly appropriate here for two reasons. First, the radiation and tidal potentials are maximum in the antisunward direction; thus circular orbits starting on the positive x -axis have larger Jacobi constants than circular orbits of the same radius starting elsewhere. Our results for circular orbits, therefore, are conservative in the sense that at each distance, we study the initially circular orbit that, energetically, has the least chance of escaping. The second reason that our initial conditions are reasonable is more physical. One of the most dangerous potential sources for material in the circumasteroidal environment is a ‘‘feeder’’ satellite, a small body from which material can be efficiently removed by meteoroid bombardment (Burns and Hamilton 1992). In contrast to direct impacts on the central asteroid in which material generally escapes or is reaccreted, much of the debris blasted from a moonlet can end up in orbit around the asteroid. We envision the following scenario: a ‘‘feeder’’ satellite uninfluenced by radiation pressure is continually subjected to a flux of hypervelocity particles which blasts debris from its surface. Although sufficiently energetic to escape the weak gravity of the satellite, much of the debris cannot escape

the asteroid. As the clumps of ejected material separate exposing small bodies to solar rays, radiation pressure begins to exert its influence, preferentially eliminating the smaller particles. Our integrations begin at the point when mutual gravitational and shadowing effects can be neglected; further evolution of the debris in the aftermath of an impact event is governed by Eq. (13).

Confining ourselves to an orbit of a given starting inclination, we still must fix the initial size of the particle's circular orbit as well as the strength of the radiation pressure as parameterized by γ ; thus we have a two-parameter space to explore. In order to avoid confusion, we continue to display plots for "Amphitrite" with distances measured in asteroid radii and particle sizes measured in millimeters; to apply these plots to "Gaspra" (with $e = 0$) we simply multiply the vertical axis by the ratio of the semimajor axes $2.2/2.55 \approx 0.86$ (Table I) and change "millimeters" to "centimeters." The change in the vertical axis comes from scaling distances with the size of the Hill sphere (HB1) while that of the horizontal axis arises from the condition that the parameter γ , defined in Eq. (15), be unaltered; keeping γ constant is equivalent to requiring that the product of the asteroid and particle radii be constant as was discussed immediately following Eq. (14). Most of the equations to follow, however, depend on the dimensionless quantities r (measured in Hill radii) and γ ; use of these quantities both simplifies the appearance of the equations and facilitates scaling to other asteroids. The size of the Hill sphere for "Amphitrite" and "Gaspra" in asteroid radii is given in Table I; below we make the connection between γ and the particle's size more apparent. Assuming spherical particles with the same density as that assumed for the asteroid ($\rho = 2.38 \text{ g/cm}^3$) and a radiation pressure coefficient of unity ($Q_{pr} = 1$), we find, using Eqs. (12) and (15), that γ is inversely proportional to the particle's radius; for "Amphitrite"

$$\gamma = 0.0673/s, \quad (17a)$$

while for "Gaspra"

$$\gamma = 0.673/s, \quad (17b)$$

where s is the particle's radius in centimeters.

3.3.1. Prograde orbits. Figure 9 shows the fate of several hundred prograde paths followed for five orbits of "Amphitrite" around the Sun. The picture is remarkably regular; orbits that share a common fate cluster together in one of three distinct regions with few exceptions. The relative strength of radiation pressure increases from right to left as the particle's size is decreased: this causes the rapid disappearance of bound orbits. For 10-mm particles, the division between bound and escape orbits is in agreement with that found analytically and numerically

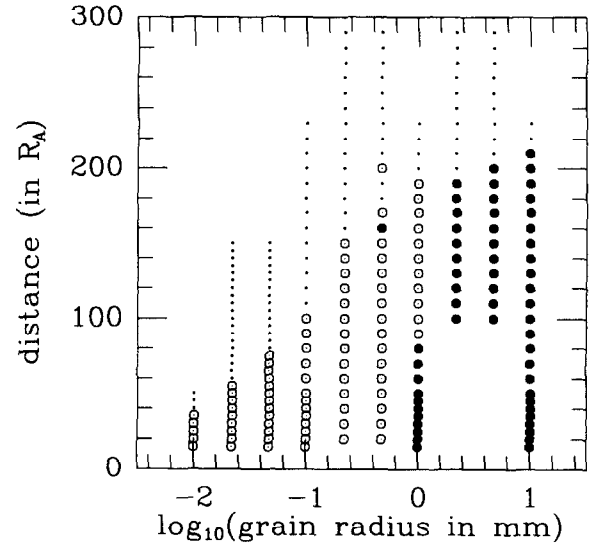


FIG. 9. The fate of approximately 200 particles of different radii started on *prograde* circular orbits of various sizes that evolve under the influence of solar radiation pressure; symbols are defined in Fig. 2's caption. The columns of initial conditions are evenly spaced along the horizontal axis. Orbits with the same fate tend to cluster, dividing the plot into three distinct regions. Note the rapid disappearance of bound orbits as the particle sizes are reduced to 1 mm and then to ≈ 0.5 mm. This, of course, is due to the increasing strength of radiation pressure relative to the asteroid's gravity. For "Gaspra," corresponding particle sizes would be 10 times larger.

by HB1 in the absence of radiation pressure: initially circular prograde orbits are stable out to about $220 R_A$, or about one-half the radius of the Hill sphere. In this region, radiation pressure is strong enough to perturb orbits, but does not have the power to alter the orbital fates of many particles. As particle sizes are decreased, increased radiation pressure is seen to cause only a few extra escapes at large distances from the asteroid until we consider particles with radii of a millimeter. In the 1-mm column of Fig. 9 an amazing transition takes place; bound orbits suddenly extend only half as far from the asteroid as they did for particles twice as large, their demise being due to the appearance of a large number of orbits doomed to strike the asteroid. For these particles, radiation pressure is large enough to induce major oscillations in orbital eccentricity, excursions so large that $e \rightarrow 1$ and a collision with the minor planet occurs. Even more startling is the disappearance of bound orbits in the next column to the left; all orbits beyond $20 R_A$, with one exception, either impact the asteroid or escape from its gravitational grasp. Particles in this column have radii ≈ 0.5 mm; around "Gaspra" this corresponds to particles nearly a centimeter across! Decreasing particle sizes still further yields no surprises; bound orbits do not reappear, and the increasing radiation pressure causes escapes to occur ever closer to the asteroid. Recall that all of the points plotted in Fig.

9 correspond to the fates of particles followed for just over 20 years; for this problem, radiation pressure accomplishes much in an extraordinarily short amount of time!

Probably the most interesting portion in Fig. 9 is the transition region where orbits first begin to impact the asteroid. Examining the orbits of the eleven 1-mm grains that crash, we find all but three of them, the one closest to the asteroid and the two furthest from it, impact in about a third of an asteroid year. Orbital eccentricities rise monotonically to a critical value near unity at which point the pericenter of the orbit dips below the surface of the asteroid and impact occurs. The three exceptions, however, show that this is not the full story. Two of these orbits survive one stint of large eccentricity after which the orbit circularizes and the process begins anew. These orbits crash when the eccentricity rises to values near one a second time. The third orbit, which is the furthest from the asteroid, survives no less than eight successive periods of large eccentricity before finally striking the asteroid during its ninth cycle.

Several effects can cause these deviations from the simple sinusoidal oscillations of eccentricity predicted by Mignard (1982). Since the orbits under discussion are large, the tidal force from the Sun is significant and cannot be ignored as it is in the idealized case. This force will also influence the orbital eccentricity and may either augment or detract from radiation-induced changes. Furthermore, even in the absence of the tidal force, orbits of this size have long periods for which the orbital averaging employed by Burns *et al.* (1979) and Mignard (1982) is generally inappropriate. This will be the case any time the particle's orbital elements change significantly during a single circuit around the asteroid. One important consequence of rapidly varying elements is that if a particle attains an eccentricity of one at some point far from the asteroid, the eccentricity may decrease below the critical value necessary for collision before the particle suffers a close approach. This, in fact, is the reason that the three orbits just discussed survive several close approaches. A final consideration that does not affect our integrations, but would alter orbits around a real asteroid, is the non-spherical shape of typical minor planets. Higher-order gravity terms can significantly alter the evolution of even a large orbit if, as in the case under discussion, the eccentricity of the orbit is near unity so that close approaches occur.

The fish shape plotted in rotating coordinates in Fig. 10 is the amazing orbit discussed above that narrowly avoids collision eight times only to impact the asteroid on the ninth pass. The heavy black line is the zero-velocity curve appropriate for the initial condition, a 1-mm particle starting on a circular unperturbed orbit around the asteroid "Amphitrite" at $190 R_A$. Although the ZVC is open, the particle never had the chance to taste the freedom of

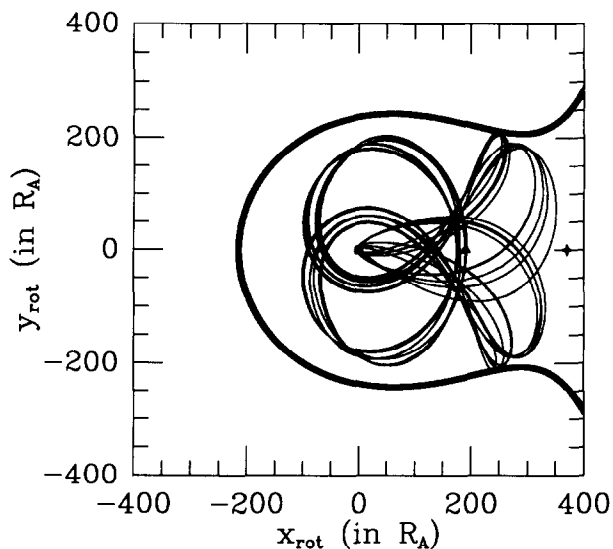


FIG. 10. A 1-mm particle on an initially circular *prograde* orbit started at $190 R_A$. The initial position is marked with a solid triangle whose upper apex points in the direction of the initial velocity; a filled square marks the end of the integration, and a solid circle represents the asteroid itself. In this case, the square and the circle overlap since the grain ends its orbital evolution on the asteroid's surface. The four-pointed star is the equilibrium point, and the heavy curve partially enclosing the orbit is the zero-velocity curve appropriate for this initial condition; its asymmetry is due to radiation pressure. Although the ZVC shows that the particle is energetically able to escape, the grain suffers a more drastic fate.

heliocentric space. At first sight this is strange, since the orbit extends nearly to the Lagrange point where forces on a stationary particle balance; *prograde* orbits that reach this far invariably escape since the Coriolis acceleration is outwardly directed. *Retrograde* particles, however, are stabilized by the Coriolis acceleration and can safely wander in this region; closer inspection of Fig. 10 reveals that although the orbit begins *prograde*, it becomes *retrograde* when farthest from the Sun, at the very fringes of heliocentric space. In fact, the orbit switches from *prograde* to *retrograde* and back again periodically, as can be seen from the time history of the inclination displayed in Fig. 11. These transitions necessarily take place at $e = 1$, when the particle's velocity vector points either directly toward or away from the asteroid; thus the very fact that the orbit survives so long warns us of the dangers of taking the orbit-averaged equations too seriously.

The history of the osculating elements in Fig. 11 is also enlightening, especially when discussed along with the evolution of the actual orbit. After a single *prograde* loop, the orbit switches to *retrograde* as the eccentricity approaches one; this first occurs very near the upper part of the zero-velocity surface in Fig. 10. A change in inclinations from $i = 0^\circ$ to $i = 180^\circ$ or vice versa can, but need not, involve closely approaching the ZVC; this only

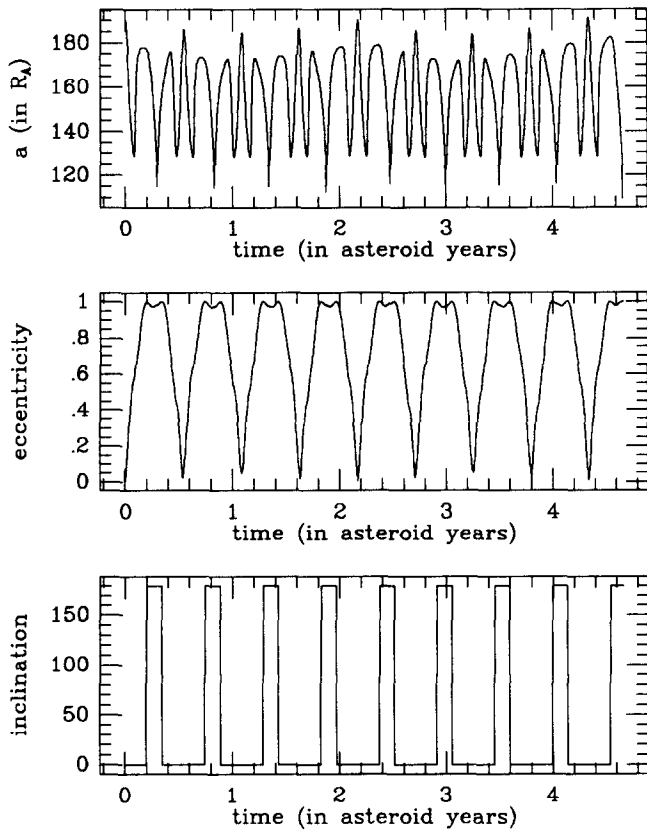


FIG. 11. The time histories of some of the osculating orbital elements for the path displayed in Fig. 10. Plotted are the orbit's semimajor axis, its eccentricity, and its inclination. These curves are calculated by integrating the equation of motion, and transforming the resulting velocity v and position r into orbital elements (Danby 1988). Note that the particle switches from prograde ($i = 0^\circ$) to retrograde ($i = 180^\circ$) and back again periodically each time the eccentricity reaches unity.

occurs if the particle is at the apocenter of a rectilinear ellipse ($e = 1$). Indeed, Fig. 10 has examples of transitions at varying distances from the ZVC. The particle then dives in for a close approach to the asteroid which occurs at the small dip in the center of the eccentricity peak. The small reduction in eccentricity, which manifests itself in less than an orbital period, is enough to allow the particle to successfully negotiate the treacherous region. The particle subsequently moves outward toward the lower part of the ZVC, finally returning to its prograde state to repeat the cycle anew. The entire cycle, in which the eccentricity changes from zero to unity and back to zero, takes only four orbits of the particle around the asteroid; clearly an orbit-averaging technique is invalid here! The inadequacy of orbit-averaging can also be seen in the semimajor axis history of Fig. 11. Orbit-averaging of both radiation pressure and the tidal acceleration lead to predictions that the semimajor axis, a , will remain constant on time scales larger than the particle's orbital period; these predictions

rely on the fact that the orbital elements, a included, do not change much during a single orbit. Large variations in the semimajor axis should, therefore, not occur on any time scale; the extent to which this is untrue is a measure of the validity of the averaging approximation.

3.3.2. Retrograde orbits. Figure 12 is the retrograde counterpart to Fig. 9. Qualitatively the two plots are very similar since radiation pressure acts analogously on prograde and retrograde orbits as is seen below; differences in the plots can be explained by the effects of the Coriolis acceleration. As in Fig. 9, orbits in Fig. 12 are segregated into three distinct regions containing bound, escape, and crash orbits. For weak radiation pressure, such as that acting on 10-mm particles, circular orbits are stable out to about the Hill sphere in accordance with the results of HB1. The Coriolis acceleration exerts a powerful influence on these orbits, keeping them bound at twice the distance of the largest prograde orbits. Retrograde orbits, like their prograde counterparts, experience a slight degradation of stability as particle sizes are decreased; but as with prograde orbits, an abrupt transition occurs for 1-mm particles: half of the bound orbits are replaced by those that crash! The rapid erosion of stability is continued for grains ≈ 0.5 mm in size for which bound orbits disappear entirely; comparing Figs. 9 and 12, we see that the disappearance of bound orbits in each case occurs for particles of the same size. As radiation pressure is increased, crash orbits continue to yield to escape orbits. Comparing with Fig. 9 again, we find a few extra crash

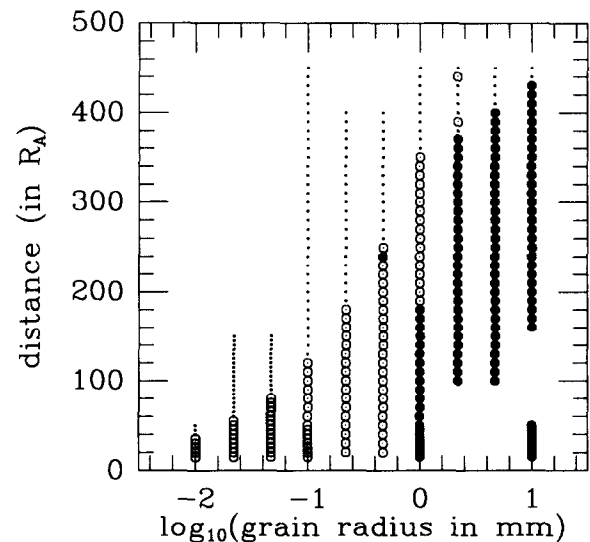


FIG. 12. The fate of about 300 particles of different radii started on retrograde circular orbits of various initial sizes. As in Fig. 9, orbits sharing a common fate cluster into three distinct regions; bound orbits rapidly disappear as particle sizes are decreased to 1 mm and then to ≈ 0.5 mm. For particles smaller than 0.1 mm, the differences between Fig. 9 and this plot are slight.

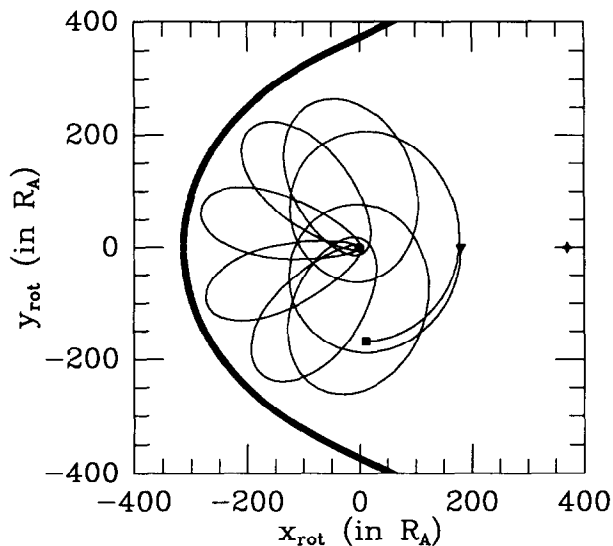


FIG. 13. A 1-mm particle on an initially circular *retrograde* path starting at $180 R_A$; symbols are those defined in Fig. 10's caption. Although the initial conditions for the particle in this figure and the one in Fig. 10 are quite similar, the orbital paths have a very different appearance. The zero-velocity curve for this initial condition is open even wider than the one in Fig. 10; the fact that the particle does not escape is an example of the poor constraint imposed by retrograde ZVCs. Only the first several loops of this orbit are shown, but subsequent motion repeats the pattern shown here.

orbits in the retrograde case which rapidly disappear as the strength of radiation pressure increases; these extra impact orbits can also be attributed to Coriolis effects.

Figure 13 shows the most distant bound orbit in the 1-mm column of Fig. 12; its initial conditions are appropriate for a grain started at $180 R_A$ from "Amphitrite." Although we show only the first eccentricity cycle, which occurs over about an asteroid year, this orbit was in fact followed for five circuits of the asteroid around the Sun. The eccentricity behavior is similar to that of the prograde orbits; it increases to a value near one, remains flat as the "ellipses" in Fig. 13 move slowly clockwise, then decreases back to zero as the particle returns roughly to its initial position. Because the orbit is almost periodic, subsequent evolution repeats that described above although the "ellipses" do not fall exactly atop those already present. In its 5-year tour, the particle survives multiple close approaches, the closest a mere 1.9 radii above the asteroid's surface! All impact orbits for 1-mm particles in Fig. 12 have the same sunwardly directed petals and general characteristics of the orbit in Fig. 13; in the former cases, however, the close approaches dip below $1 R_A$ abruptly cutting short the orbital evolution! As with the prograde orbits discussed above, most of these retrograde orbits impact midway through their first eccentricity oscillation, although three of the five furthest survive at least one cycle for reasons similar to those discussed in Section

3.3.1. Moving closer to the asteroid along the 1-mm column, we find that bound orbits have progressively more distant close approaches (corresponding to smaller eccentricities), although again the orbital shapes are reminiscent of Fig. 13. Finally, we note that all bound orbits, Fig. 13 included, are purely retrograde; further from the asteroid, however, we do encounter orbits that switch between the prograde and retrograde states. Particles on these outer orbits have short lifetimes since they invariably crash while traversing the often fatal $e = 1$ regime.

3.3.3. *Inclined orbits.* The situation for inclined orbits (here the term inclined will refer to orbits with $i = 90^\circ$) is somewhat different than for planar ones. In the orbit-averaged equations of Burns *et al.* (1979) and Chamberlain (1979) there is a $\cos i$ term that is small for inclinations near 90° but equal to ± 1 for planar orbits. The change in this term reflects simple differences in the orbital geometry which we illustrate with discussion of a hypothetical circular orbit around the asteroid. Imagine that a grain is started on a circular orbit fairly close to the asteroid such that its period is much less than that of the asteroid around the Sun. If the grain is placed on either a prograde or a retrograde orbit, the angle between the Sun and the particle as measured from the asteroid will circulate between 0° and 360° every synodic period; recall that the synodic period is the period of the particle with respect to the Sun. For a path inclined 90° to the asteroid's orbital plane, however, the situation is quite different. If the particle is started on the positive x -axis, then after one-quarter of an asteroid orbit, the direction to the Sun is everywhere perpendicular to our hypothetical unperturbed circular orbit; at this point, the angle which circulates for the planar cases is constant! Clearly radiation pressure will act differently on inclined orbits than on planar ones. Considerations of the averaged equations of motion and the fact that a perpendicular perturbing force does not affect the orbital eccentricity (Danby 1988) lead us to the conclusion that driving orbital eccentricities to large values will be more difficult in the inclined case.

Figure 14 verifies these ideas; bound orbits exist for particles approximately five times smaller than that where the last bound planar orbits are seen. These bound orbits in the transition region disappear even more abruptly than in the planar case; in the column for ≈ 0.2 -mm particles, stable orbits abound and there are no crash orbits while in the next column to the left there are no bound ones! Impact orbits sprinkled throughout the region of weak radiation pressure are probably not associated with that force at all; HB1 noted a large number of such orbits for inclinations in the near 90° range in their integrations of the purely gravitational three-body problem. Discounting these exceptions, the bound, escape, and crash orbits separate nicely into three regions as before. In Fig. 14, as

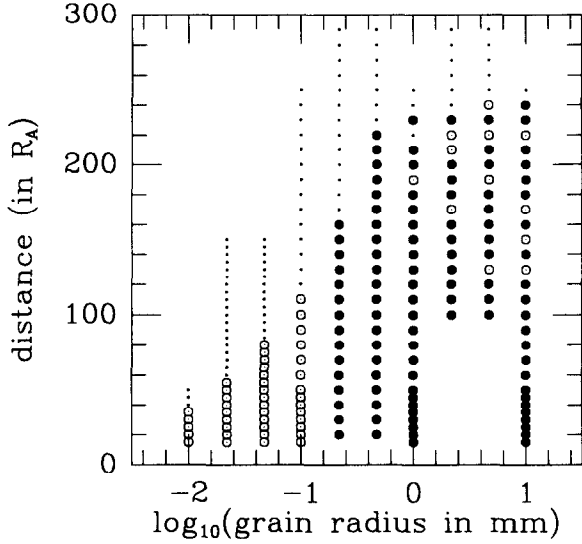


FIG. 14. The fate of approximately 200 particles of different sizes started on circular paths initially *inclined at 90°*. These orbits jealously guard their stability until particle sizes are reduced to 0.1 mm; reasons for this are discussed in the text. Crash orbits in the upper left of the diagram are of the type seen in Fig. 5 and are caused by the tidal force; those to the lower right, however, are due to radiation pressure. Comparing this figure to Figs. 9 and 12, we see few differences for particles smaller than 0.1 mm.

in the planar figures, the right side of the plot smoothly approaches results found by HBI in the absence of radiation pressure. For very small particles that are significantly influenced by radiation pressure, results are in accordance with the planar cases; there are a few more impact orbits than in the analogous columns in Fig. 9 and a few less than in Fig. 12 as could be predicted by considering the Coriolis acceleration. In this region of all three figures, orbits crash extremely rapidly; few survive more than the time necessary to increase the eccentricity to one.

3.4. Analytic Considerations

3.4.1. Bound–escape division. For each of the orbital classes (prograde, retrograde, inclined) described above, we have found that—to a greater or lesser degree—particles with similar characteristics (particle radius, initial orbit size) share similar fates, and that the boundaries between these fates are sharply defined. This suggests that the outcomes for such particles are being determined by simple processes; hence we now seek the mechanisms that segregate orbits into the three separate regions noted above. In this section and the ones to follow, we discuss the factors that cause a particle to escape and to crash, and we develop analytical expressions that define the divisions separating these areas from each other and from the region of bound orbits.

We know, by analogy with the purely gravitational case, that if orbits lie within closed ZVCs they will remain bound. Hence, as a criterion for escape, the opening of the zero-velocity curves will prove to be useful, at least in the prograde case. To connect ZVCs to the orbits discussed above, we substitute the initial conditions, $y = z = 0$ and the initial circular velocity condition,

$$v_{\text{rot}}^2 = \left(\left(\frac{3}{d_{\text{BE}}} \right)^{1/2} \cos i - d_{\text{BE}} \right)^2 - \left(\frac{3}{d_{\text{BE}}} \right) \sin^2 i, \quad (18)$$

into Eq. (14) to obtain

$$C_{\text{BE}} + \frac{3}{d_{\text{BE}}} + 2(3d_{\text{BE}})^{1/2} \cos i + 2d_{\text{BE}}^2 + 6\gamma d_{\text{BE}}, \quad (19)$$

where C_{BE} is the Jacobi constant for which the zero-velocity curves first open and d_{BE} is the critical distance at which we expect the bound-escape division to occur. We solve this equation numerically in each of the three inclination cases and plot part of the solution curve in Figs. 15–17 (dashed line). If extended to smaller particle sizes, the curve would also separate those crash orbits that had the potential to escape from those that did not. Although the theoretical results in all three inclination cases correctly predict that orbital stability is lost as particle sizes are decreased, the curves only succeed in fitting the numerical results for prograde orbits; the match stead-

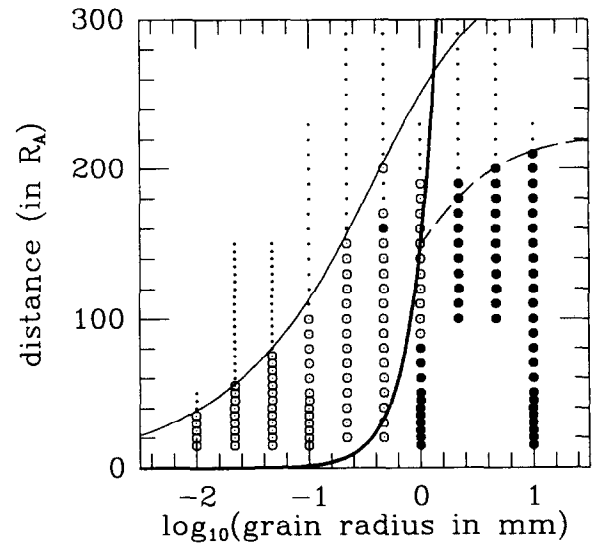


FIG. 15. *Prograde* orbits. Same as Fig. 9 but now including theoretical lines dividing bound, escape, and crash orbits. The dashed line, discussed in Section 3.4.1, presents a criterion that should separate particles that are bound from those that escape. Similarly, the heavy and lightweight solid curves are those that our theory predicts for the bound–crash (Section 3.4.2) and crash–escape (Section 3.4.3) divisions, respectively.

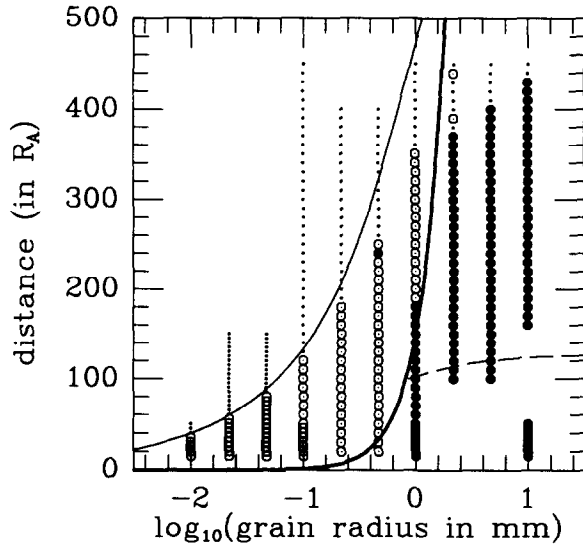


FIG. 16. *Retrograde orbits.* Same as Fig. 12 with theoretical lines dividing bound, escape, and crash orbits. See Fig. 15 and the text for an explanation of the three curves.

ily worsens as the inclination is increased. The reason for this is, of course, that the derivation of Eq. (19) ignores the all-important Coriolis acceleration. Not surprisingly, the radial portions of the neglected Coriolis term, which has a $\cos i$ dependence, provides increasing stability as the inclination is raised from $i = 0^\circ$ to $i = 180^\circ$. The situation is complicated by nonradial parts of the Coriolis acceleration, with a $\sin i$ dependence, which tend to destabilize orbits. The two effects combine to explain why the division between bound and escape orbits, as numerically

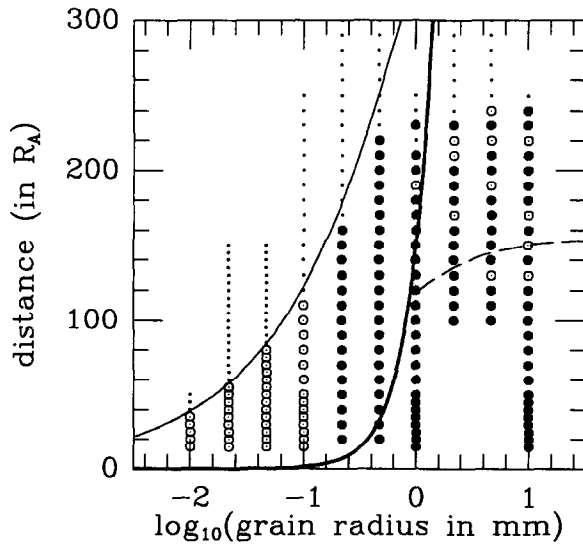


FIG. 17. *Inclined orbits.* Same as Fig. 14 with theoretical lines dividing bound, escape, and crash orbits. See Fig. 15 and the text for an explanation of the three curves.

obtained, occurs at a similar distance in the prograde and $i = 90^\circ$ cases but much further out for retrograde orbits (HB1).

3.4.2. Bound-crash division. Particles risk collision with the asteroid once their orbital eccentricities become so large that at pericenter their orbits pierce the asteroid's surface: $r_p = a(1 - e) < R_A$. If we neglect the tidal acceleration—an approximation that is certainly valid for strong radiation pressure—we can apply Mignard's expression for the eccentricity produced by radiation pressure (1982, his Eq. (28)) to determine when an impact can occur. More precisely, the tidal acceleration can be ignored in determining when escapes will occur for orbits with initial semimajor axes $\lesssim r_H/3$ since tides cause only small eccentricity oscillations in this regime. Furthermore, for orbits much larger than this, the orbit-averaging procedure employed by Mignard (1982) is no longer valid. For initially circular prograde orbits, Mignard's result for the variation of eccentricity can be rewritten in the useful form

$$(1 - e^2)^{1/2} = \frac{n^2}{\alpha^2 + n^2} + \frac{\alpha^2}{\alpha^2 + n^2} \cos [(\alpha^2 + n^2)^{1/2} t], \quad (20)$$

where α is given by the equation: $\alpha = 3/(2\tau_0)$, and τ_0 is Chamberlain's (1979) expression for the time it takes radiation pressure to produce the circular velocity, i.e., $\tau_0 = (GM_A/r)^{1/2}/(\beta GM_\odot/R^2)$. Loosely, α is the strength of the solar radiation pressure relative to the asteroid's local gravity. For weak radiation pressure ($\alpha \ll 1$), the eccentricity simply varies with the solar period, while for strong radiation pressure e varies more rapidly. Although mathematically Eq. (20) predicts a complex eccentricity when the right-hand side of the equation is less than zero (i.e., when $\alpha > n$ and $\cos < 0$), this does not actually occur in the orbit-averaged perturbation equations from which Eq. (20) is derived because e is prevented from exceeding unity by $1 - e^2$ terms in these equations. What, then, really happens as e approaches one? There are two possibilities: the particle either can collide with the asteroid, preventing further evolution of the orbital elements, or, for longer-lived orbits, a prograde-to-retrograde transition can take place. Because Mignard's solution is restricted to prograde orbits, it is unable to predict the prograde-to-retrograde transition and instead suggests a complex eccentricity.

It is not difficult to repeat Mignard's derivation for retrograde orbits. We begin with the orbit-averaged equations of motion and consider the planar limit $i = 180^\circ$ (instead of the $i = 0^\circ$ taken by Mignard). With an appropriate choice of variables, the form of the resulting pair of equations can be made identical to those for the prograde case; specifically, we find that Eq. (20) applies equally well to retrograde orbits. This is a single example of a

more general result: if the orbital elements, evolving under some perturbation force, are taken to remain constant over a single sidereal period, then the resulting orbit-averaged equations will yield similar histories for prograde and retrograde orbits. According to this model of the effects of radiation pressure, therefore, there should be no difference in the fate of initially circular prograde and retrograde orbits since Eq. (20) governs the evolution of both. This is true, of course, only as long as the particle remains close to the asteroid where the Coriolis acceleration, which encapsulates the differences between prograde and retrograde orbits, can be ignored. Further from the asteroid, differences in the Coriolis acceleration manifest themselves in the increased stability of the retrograde particles noted in the discussion of Figs. 9 and 12. In these regions (e.g., 1-mm crash orbits), Eq. (20) does not strictly apply.

A collision with the asteroid can occur when the pericenter of the osculating orbit dips below the asteroid's surface. For the large orbits under discussion, this requires an eccentricity that is nearly unity. Accordingly, we solve for the minimum α that allows $e = 1$ in Eq. (20); although e cannot exceed one, it must necessarily attain this value during a prograde-to-retrograde transition. The collision criterion is $\alpha = n$, which can be recast as

$$d_{\text{BC}} = \frac{4}{27\gamma^2}, \quad (21)$$

where d_{BC} is the dimensionless critical distance at which the division between bound and crash orbits is located. Furthermore, near this division where, by definition, $\alpha \approx n$, we expect that collisions will occur in half the period given by Eq. (20), i.e., $2^{-3/2} \approx 0.35$ asteroid years. This simple estimate is in very good agreement with the $\frac{1}{3}$ of a year observed for the prograde orbits discussed in Section 3.3.1. Equation (21) is also plotted on each of Figs. 15–17 as a solid, heavyweight curve. We find reasonable agreement in the prograde and retrograde figures, but a rather poor match for the inclined orbits. The fact that inclined orbits are more resistant to radiation pressure-induced impacts should not be surprising in light of the discussion in Section 3.3.3. For 1-mm particles around “Amphitrite” where the limits of the theory are stretched the most, we see that bound retrograde orbits extend further from the asteroid than expected (Fig. 16), while bound prograde orbits extend to distances less than predicted (Fig. 15). These differences, which are due to the neglected Coriolis acceleration, only appear for large orbits.

For ≈ 0.5 -mm particles, bound orbits do not extend as far as predicted in both the prograde and retrograde cases. This is due to the finite size of the asteroid which allows impacts to occur for eccentricities less than one. This effect can be derived from Eq. (20) by putting $e = e_{\text{crash}}$,

where $e_{\text{crash}} = 1 - R_A/d_{\text{BC}}$. Setting the cosine to -1 , and solving for α/n as before, we find

$$d_{\text{BC}} = \frac{4f^2(e_{\text{crash}})}{27\gamma^2}, \quad (22)$$

where $f(e_{\text{crash}})$ is given by

$$f(e_{\text{crash}}) = \frac{1 - (1 - e_{\text{crash}}^2)^{1/2}}{e_{\text{crash}}}; \quad (23)$$

and $f^2(1) = 1$ so that Eq. (21) is recovered. The solution of Eqs. (22) and (23) is complicated since e_{crash} is a function of d_{BC} ; in general, the equation must be numerically solved. In practice, however, an iterative procedure in which an initial value of d_{BC} is substituted into the right-hand side of Eq. (22) to compute an updated value converges to a reasonable estimate relatively rapidly. As an example, consider the bound–crash division for ≈ 0.5 -mm particles which Eq. (21) predicts will occur at about 30 asteroid radii. For this distance, a collision takes place when $e = e_{\text{crash}} = 29/30 \approx 0.97$ for which $f^2(0.97) \approx 0.59$! Thus instead of occurring at 30 asteroid radii, a single iteration of Eq. (22) predicts that the division should happen at about 18 asteroid radii; a few more iterations show that the division is actually nearer to 14 R_A which is in good agreement with the data in Figs. 15 and 16. The surprisingly large change in $f^2(e_{\text{crash}})$ for $e_{\text{crash}} \lesssim 1$ has its origins in the fact that radiation pressure takes a long time to further increase the eccentricity of an already highly eccentric orbit.

To make our results more useful, we instead solve for the minimum-sized particle found in an asteroid's neighborhood by applying Eq. (22), and employing Eqs. (12) and (15) to return to more familiar dimensional units. We find that particles satisfying the following inequality

$$\left(\frac{s}{1 \text{ cm}}\right) \leq \left(\frac{1}{120f(e_{\text{crash}})}\right) \left(\frac{r}{1 R_A}\right)^{1/2} \left(\frac{M_{\text{Amphitrite}}}{M_{\text{Asteroid}}}\right)^{1/3} \\ \times \left(\frac{2.55 \text{ AU}}{a}\right)^{1/2} \left(\frac{Q_{\text{pr}}}{1.0}\right) \left(\frac{2.38 \text{ g/cm}^3}{\rho}\right) \quad (24)$$

are removed from circumasteroidal orbit. This formula is applicable only for strong radiation pressure where the bound–crash division exists (see Figs. 15 through 17), roughly where $\gamma \geq 1$. We find for “Gaspra” that, outside of 10 R_A , no particles with $s \leq 0.45$ cm should be found and at Galileo's flyby distance of $\approx 200 R_A$, all particles with $s \leq 1.4$ cm should be absent. [Note added in revision: Grün *et al.* (1991) report that Galileo's dust instrument, sensitive to particles larger than 0.1 μm , detected no hits during its encounter with Gaspra.]

3.4.3. Crash–escape division. Although the criteria described in the two preceding sections define the most interesting boundaries, namely those that separate regions where particles can freely orbit from regions where they cannot, we now derive, for completeness, an approximate argument to describe the curve separating orbits that crash from those that escape. Unlike the boundaries discussed in the previous sections, here there is no nice theory to appeal to so we make the following somewhat arbitrary choice. We say that if a highly perturbed particle can complete a single orbit around the asteroid, its eventual fate will be to crash into the asteroid. While this is not always true (some orbits near the actual boundary complete a few loops before escaping), it does apply to most of our numerical results, especially those for strong radiation pressure. We approximate further by saying that if our particle has enough “energy” to complete a quarter of a hypothetical circular orbit, it will complete a full loop around the asteroid and hence will eventually crash. This statement is certainly approximate since the path actually followed by the particle is certainly not circular; a look at the shape of the orbits in Figs. 10 and 13, however, shows that the approximation is fairly reasonable. In any case, particles with significantly less energy have no hope of swinging around the asteroid, while those with more “energy” should be able to. Mathematically, we set the right-hand side of Eq. (14), evaluated at $(x, y, z) = (d_{CE}, 0, 0)$ with v_{rot} as given by Eq. (18), equal to the same expression evaluated at $(0, d_{CE}, 0)$ with $v_{rot} = 0$. The result is

$$\frac{3}{d_{CE}} = 2(3d_{CE})^{1/2} \cos i + 2d_{CE}^2 + 6\gamma d_{CE}, \quad (25)$$

where d_{CE} is the distance to the division between crash and escape orbits. We numerically solve Eq. (25) to obtain the last defining curve which is plotted in Figs. 15–17 as a solid, lightweight curve. This approximate division agrees remarkably well with the actual boundary for strong radiation pressure, deviating significantly only for large orbits along which the neglected tidal and Coriolis accelerations are important.

4. DISCUSSION

The above calculations and those of other groups have been carried out not so much to solve new celestial mechanics problems but rather to address a practical question: will the circumasteroidal environment be hazardous to a flyby spacecraft? Accordingly, a reader might anticipate that we would conclude this paper with a probability calculation determining the odds of finding debris of various types in the asteroid’s neighborhood. Unfortunately such calculations are fraught with uncertainty since they involve complicated supply and loss mechanisms, many

of which are poorly constrained. We therefore content ourselves with a qualitative description of this problem, summarizing possible supply and loss processes.

As pointed out by Chauvineau and Mignard (1990a), HB1, and many others, the distance within which coplanar prograde material can remain trapped for short periods about an asteroid circling the Sun is roughly half the Hill radius; for coplanar retrograde particles the size increases to about a full Hill radius. In extending these ideas to three dimensions, HB1 showed that bound out-of-plane material can only rise to about two-thirds of a Hill radius; they used their results to define a stability surface within which bound orbiting material might be found. This surface overestimates the zone of stability, however, because nearly all unmodeled processes, some of which operate on short time scales and others that take ages, are destabilizing. The former dominate, since they will overwhelm continuous supply mechanisms, which act on longer time scales. Accordingly, the focus of this paper has been to discuss the effects that cause changes to the stability of orbits in time intervals comparable to the asteroid’s orbital period (cf. Burns and Hamilton 1992).

In assessing the importance of an asteroid’s elliptical orbit on the size of the stability zone, we discovered that the dimensions of the zone are roughly proportional to the minimum asteroid–Sun distance. Since the effects of an elliptic orbit can be quantified, the safety of a passing spacecraft can be assured simply by avoiding an asteroid’s calculated stability zone. We also found that radiation pressure is remarkably effective in sweeping small particles rapidly out of the circumasteroidal environment. These grains would normally be expected to be the most numerous and, since the largest of them can severely damage a spacecraft, they pose the greatest threat to a flyby mission. Since small grains are removed much more rapidly than they are resupplied, however, our results define a region of space in which small orbiting debris will not be found.

Many loss mechanisms operate over much longer time scales. In this category we include the long-term effect of the gravitational tugs of Jupiter and the other planets (Chauvineau and Mignard 1990b) as well as close approaches of other asteroids which can disrupt a binary pair (Chauvineau *et al.* 1991). These effects cause particles within the stability zone defined above to escape, but their efficiency is critically dependent on the unknown rate at which supply mechanisms populate the stability zone. Other long-term loss processes—notably Poynting–Robertson drag, catastrophic fragmentation, and sputtering—act most effectively on small grains. These grains are more efficiently removed by radiation pressure; collisions, for example, set lifetimes at $\sim 10^4$ – 10^5 years for particles between tenths of millimeters and centimeters in radius while radiation pressure typically removes such grains in only a few years. The

important point to make is that *all* of these loss processes cause the actual region of space filled by stable orbits to be smaller than a simple circular three-body model would suggest.

Several mechanisms (Weidenschilling *et al.* 1989, Burns and Hamilton 1992) might supply circumasteroidal satellites or debris: (i) primordial coaccretion processes like those that are believed to have produced most planetary satellites; (ii) formation in a nearly catastrophic collision like the event thought to have generated Earth's Moon; (iii) capture of interplanetary debris within the asteroid's stability zone; (iv) a continuous flux of impact ejecta leaking off the asteroid itself as the latter is bombarded by micrometeoroids; and (v) similar ejecta leaving an asteroidal "feeder" satellite. The last of these is thought to be the most feasible supplier of circumasteroidal debris, since a significant fraction of the ejecta can remain trapped in this case in contrast to mechanism (iv). Unfortunately it is also the least calculable!

Since none of these processes can be quantified well and since definitive observations of life-threatening debris cannot be made from the ground, mission planners have been quite anxious about where in the vicinity of an asteroid a spacecraft could safely fly. Clearly this is a very difficult engineering question. Nonetheless, within the assumptions of the models, the recent research summarized above shows that regions beyond a few hundred asteroid radii will not contain stably trapped particles and that small particles will be entirely absent from asteroid's vicinity. In addition, it is encouraging that no schemes seem capable of populating the most distant stable orbits. Nevertheless, when entering unknown territory, one always has a nagging worry that something was ignored, perhaps a new mechanism to stabilize orbits or one to efficiently generate distant material. For that reason these authors, at least, have greeted the unscathed flight of the Galileo spacecraft past 951 Gaspra at a distance of $\sim 200 R_A$ with a sigh of immense relief.

ACKNOWLEDGMENTS

We thank Philip Nicholson for critically reading an earlier version of this text, as well as Myron Lecar and an anonymous reviewer for commenting on the paper. JAB thanks Joseph Veverka for overseeing the selection of referees and for making editorial decisions on this paper.

REFERENCES

BURNS, J. A., AND D. P. HAMILTON 1992. Debris about asteroids: Where and how much? *Asteroids, Comets Meteors III*, in press.

- BURNS, J. A., P. L. LAMY, AND S. SOTER 1979. Radiation forces on small particles in the Solar System. *Icarus* **40**, 1–48.
- CHAMBERLAIN, J. W. 1979. Depletion of satellite atoms in a collisionless exosphere by radiation pressure. *Icarus* **39**, 286–294.
- CHAUVINEAU, B., AND F. MIGNARD 1990a. Dynamics of binary asteroids. I. Hill's case. *Icarus* **83**, 360–381.
- CHAUVINEAU, B., AND F. MIGNARD 1990b. Dynamics of binary asteroids. II. Jovian perturbations. *Icarus* **87**, 377–390.
- CHAUVINEAU, B., P. FARINELLA, AND F. MIGNARD 1991. The lifetime of binary asteroids vs gravitational encounters and collisions. *Icarus* **94**, 299–310.
- DANBY, J. M. A. 1988. *Fundamentals of Celestial Mechanics*. 2nd ed. Willmann-Bell, Richmond, VA.
- GRÜN, E., AND 12 COLLABORATORS 1991. Interplanetary dust observed by Galileo and Ulysses. *Bull. Am. Astron. Soc.* **23**, 1149.
- HAMILTON, D. P., AND J. A. BURNS 1991. Orbital stability zones about asteroids. *Icarus* **92**, 118–131.
- HÉNON, M., AND J. M. PETIT 1986. Series expansions for encounter-type solutions of Hill's problem. *Celest. Mech.* **38**, 67–100.
- LECAR, M., F. A. FRANKLIN, AND P. SOPER 1992. On the original distribution of the asteroids. IV. The stability of orbits in the outer asteroid belt. *Icarus*, in press.
- LUK'YANOV, L. G. 1984. Coplanar solutions in the photogravitational restricted, circular three-body problem. *Sov. Astron.* **28**, 462–465.
- LUK'YANOV, L. G. 1986. Stability of Lagrangian points in the restricted, photogravitational three-body problem. *Sov. Astron.* **30**, 720–724.
- LUK'YANOV, L. G. 1988. Zero-velocity surfaces in the restricted, photogravitational three-body problem. *Sov. Astron.* **32**, 682–687.
- LUNDBERG, J., V. SZEBEHELY, R. S. NEREM, AND B. BEAL 1985. Surfaces of zero velocity in the restricted problem of three bodies. *Celest. Mech.* **36**, 191–205.
- MIGNARD, F. 1982. Radiation pressure and dust particle dynamics. *Icarus* **49**, 347–366.
- MIGNARD, F., AND M. HÉNON 1984. About an unsuspected integrable problem. *Celest. Mech.* **33**, 239–250.
- MILANI, A., A. NOBILI, AND P. FARINELLA 1987. *Non-gravitational Perturbations and Satellite Geodesy*. Hilger, Bristol.
- OVENDEN, M. W., AND A. E. ROY 1961. On the use of the Jacobi integral of the restricted three-body problem. *Mon. Not. Astron. Soc.* **123**, 1–14.
- PEALE, S. J. 1986. Dust belt of the Earth. *J. Geophys. Res.* **71**, 911–933; see also *J. Geophys. Res.* **72**, 1124–1127.
- SCHUERMAN, D. W. 1980. The effect of radiation pressure on the restricted three-body problem. In *Solid Particles in the Solar System* (I. Halliday and B. A. McIntosh, Eds.), pp. 285–288.
- SZEBEHELY, V., AND G. E. O. GIACAGLIA 1964. On the elliptic restricted problem of three bodies. *Astron. J.* **69**, 230–235.
- WEIDENSCHILLING, S. J., P. FARINELLA, AND V. ZAPPALÀ 1989. Do asteroids have satellites? In *Asteroids II* (R. P. Binzel, T. Gehrels, and M. S. Matthews, Eds.), pp. 643–658. Univ. Arizona Press, Tucson.
- ZHANG, S. P., AND K. A. INNANEN 1988. The stable region of satellites of large asteroids. *Icarus* **75**, 105–112.